

UNIVERSITY OF READING
Department of Mathematics
Mathematical and Numerical Modelling of Atmosphere and
Oceans MSc

**A Moving Mesh Approach to Modelling the
Grounding Line in Glaciology**

Josie Dodd

August 2013

A dissertation submitted in partial fulfilment of the requirement for the degree of Master of
Science

Acknowledgements

Firstly I would like to thank my father, Paul Dodd whose love and generosity has made it possible to complete this course. Secondly I would like to thank my project supervisor Prof. Mike Baines for all of his patience and invaluable advice.

Declaration

I confirm that this is my own work, and the use of all material from other sources has been properly and fully acknowledged.

Signed Date.....

Abstract

This dissertation aims at enhancing the understanding of glacier flow dynamics. We are primarily concerned with the behaviour of the interface between grounded and floating ice commonly referred to as the grounding line. Accurate modelling of the grounding line is integral to forecasting the fate of the cryosphere and the Earth's climate system.

In this dissertation we discuss the use of a particular moving mesh numerical scheme in modelling the flow dynamics of the grounding line. This scheme incorporates conserved mass fractions in order to move the grid nodes. The approach allows the model to maintain physical properties such as local mass balance.

We assess the ability of the method at accurately modelling the grounding line and compare the results with available literature. We also discuss future possible developments to the model.

Contents

1	Introduction	1
1.1	The Grounding Line	1
1.2	Previous Work	2
1.3	The Governing Equations	3
1.3.1	The Ice Sheet	5
1.3.2	The Ice Shelf	5
1.3.3	Interface Condition	6
1.3.4	Total Mass Balance	7
1.4	Outline of the Dissertation	7
2	Ice Diffusion Only	9
2.1	Ice Sheet	9
2.2	Ice Shelf	10
2.3	Numerical Approximations	10
2.3.1	Ice Sheet	11
2.3.2	Ice Shelf	11
2.3.3	Advancement of x and Recovery of h	14
3	Combining the Ice Sheet and Ice Shelf	16
3.1	Mass Fractions	16
3.2	Deformation Velocities	17
3.3	Numerical Approximations	18
3.3.1	Time Stepping	19
3.3.2	Recovering h	19
3.3.3	Algorithm	19
4	Adding the Source Term	21
5	Non-Dimensionalisation	23
5.1	Sheet	23
5.2	Shelf	24
6	A 1D Test Case	25
6.1	Steady State	25
6.2	Viscosity	26

6.3	Convergence	27
6.4	Velocity	29
6.5	Dependency on the Number of Nodes	29
6.6	Running Time of Model	30
7	Changes to the Accumulation Rate	31
8	Introducing a Tilt	33
9	Changes to Sea Level	41
10	Changes to Rate Factor	41
11	Conclusion and Discussion	43
11.1	Further Work	46
11.1.1	Full Stokes Equations	46
11.1.2	Higher-Dimensions	46
11.1.3	Ice Calving at the Shelf Front	47

1 Introduction

Understanding the dynamics of marine ice sheets has been a subject of increasing interest over recent years. The evolution of such marine ice sheets can have the utmost effect on the natural environment and human civilisation. Antarctica and Greenland hold enough ice to raise global sea levels by 70m [6]. Due to recent advances in the technology of satellite measurements extensive advancements have been seen in the ability to observe the Earths polar regions. There have been some alarming trends uncovered by the observations made with these recent advancements. The West Anatarctic Ice Sheet (WAIS) lost between 47 and 59 Gt (gigatonnes) of ice per year in the 1990s [2]. The WAIS alone is an ice sheet large enough that if it were to collapse entirely there could be a rise in sea level of more than 5m. It has been observed that in areas of fast flowing ice in the WAIS the reduction in ice is much greater than any change in the rate of melting or the decrease in the amount of snow can account for. This would indicate that the mass loss is a result of the glacier dynamics [6].

1.1 The Grounding Line

The grounding line of a glacier can be described as the point where the glacier shifts from being grounded to being afloat. The grounded part of the glacier is referred to as the ice sheet and the floating part of the glacier is referred to as the ice shelf. (See figure 1).

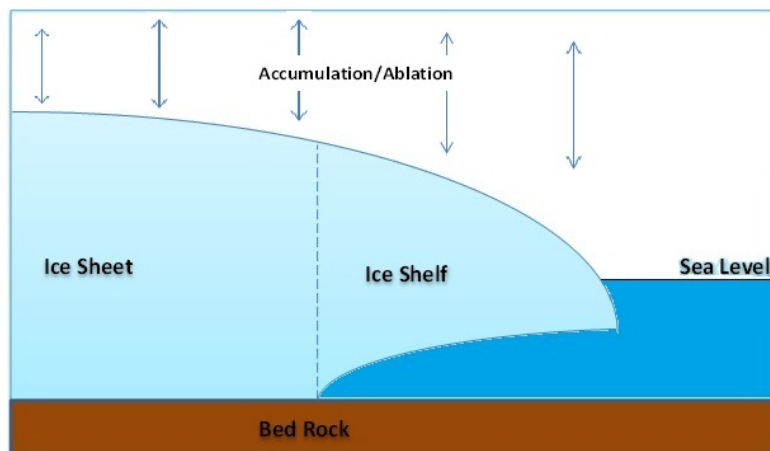


Figure 1: Illustration of Glacier

The glacier begins to float when there is enough water to support the weight of the ice. This is known as the condition for flotation and can be described by the equation

$$\rho_i h = \rho_w (l - b),$$

where ρ_i is the density of the ice, ρ_w is the density of sea water, h is the ice thickness, l is the sea level and b is the elevation of the ice base [11].

The position of the grounding line is dictated by its surrounding conditions and thus as the conditions change so too does the position of the grounding line.

The complexity of glacier dynamics is such that a purely analytical approach to modelling the grounding line is impossible. This gives rise to a distinct need for the use of numerical approximations to simulate the behaviour of the glacier. The use of computers and programming software is integral to this. The dynamics of grounding lines in glaciers has been closely examined in a variety of computational models where results are often inconsistent [2], with occasionally spurious projections as to the time frame for which ice sheets will melt. It is clear that more work in finding a suitable method of simulating the glacier dynamics is essential in order to obtain consistent results.

This dissertation aims at simulating the migration of the grounding line in glaciology using a local conservation based moving mesh technique applied to a simple model of a glacier using the shallow ice approximation.

1.2 Previous Work

It is of interest to model the progress of the grounding line because if the grounding line advances or recedes this can cause significant rises in sea levels. As ice shelves are perfectly buoyed up by the ocean according to Archimedean Principle, any contribution to sea level change is entirely due to changes in the mass of the grounded ice sheet [2]. It is important to understand what affects the behaviour of the grounding line and to establish an effective model to simulate the grounding line migration in order to predict future sea level changes. Although ice sheet models are well established there have been relatively few attempts at accurately modelling the grounding line migration and even fewer attempts at modelling the grounding line using the full Stokes' approximations: many models use a shallow ice approximation [5]. The shallow ice approximation uses a simplified version of the full Stokes' approximations where values have been vertically averaged. There was only one attempt in the MISMP survey paper [5] that used full Stokes equation.

The majority of the attempts at modelling the grounding line have so far been inconsistent. A cause of these inconsistencies could be attributed to the differing

methods of treating the coupling between the sheet and shelf and what continuity conditions are applied at the grounding line. Many models only examine the ice dynamics of the grounded ice sheet without the coupling of the floating ice shelf [11]. Hindmarsh, 1996 [3] suggests that it is possible to model the grounding line dynamics without any coupling between the sheet and the associated shelf. However, there are other models that examine the grounded ice sheet with the inclusion of coupling between the sheet and the ice shelf. The coupling can either involve full mechanical coupling between sheet and shelf using an ice stream model or a semi-coupling where only the ice flux through the grounding line is considered. This dissertation aims at examining the ice sheet with the inclusion of semi-coupling between the ice sheet and ice shelf.

Another contribution to the inconsistencies of the various models is their sensitivity to the resolution and the robustness of the numerical implementation. There are a number of methods that use fixed grid techniques. These have a rigid unmov- ing structure and are by far the simplest to implement and best understood. These methods often strongly depend on the grid size, as features may exhibit sharp changes that can only be truly represented with a grid fine enough to capture them. The grounding line in particular is a feature that requires a fine resolution for reliable results. This, however, is computationally costly. An alternative method to gain higher resolution without the extensive computational cost is to consider adaptive mesh techniques. These techniques apply a finer mesh around the grounding line and allow a coarser resolution elsewhere, thus saving computational time. A third approach uses a moving mesh technique which allows the grid points (including the position of the grounding line) to be moved. Moving mesh techniques are considered more robust and reliable, as the grounding line is part of the solution and no inter- polations are required [5]. The survey paper of Vieli and Payne [11] goes into detail of how the results differ between various numerical models with different numerical properties and we will make frequent references to this paper to compare our results.

1.3 The Governing Equations

Ice can be treated as an extremely viscous fluid, which generally deforms under its own weight over a period of time, subject to mass gain and loss at the surface of the glacier due to snowfall or melting [7]. Generally the amount of accumulation (or snow) at the upper part of the glacier is greater than the amount of ablation (loss of mass through melting), and so the mass of this region is expected to increase over time. Further down the glacier near the shelf, the rate of accumulation is less than the rate of ablation and so the mass is expected to decrease in this region. If it is

assumed that the ice spreads unidirectionally then ice will spread over the glacier as ice is pushed from the sheet towards the shelf. The total flux of ice between the sheet and the shelf is what we want to model in order to gain an idea about the behaviour of the grounding line.

It is convenient to make several assumptions in order to simplify the physical model. The key assumptions are as follows:

- The model uses the Shallow Ice Approximation, as defined below
- The bed is flat with no isostasy, (i.e. the ice sheet is not elevated or lowered in order to meet equilibrium with the Earth's crust after change in mass.)
- Temperature and density are constant
- There is no basal sliding

The mass balance equation in the shallow ice approximation is taken to be [11]:

$$h_t + (hu)_x = m. \quad (1)$$

in the time dependent region $0 \leq x \leq b(t)$, where $x = 0$ is the fixed boundary at the ice divide (the top of the glacier), $b(t)$ is the moving boundary at the shelf front, $h(x, t)$ is the height of the ice sheet, $u(x, t)$ is the diffusive velocity, and $m(x)$ is the accumulation rate. The accumulation term represents the combination of mass gain from snow and mass loss from ablation.

The boundary conditions for this problem are that there is no flux at the fixed boundary $x = 0$ and so $u = 0$ at this point and also there is zero total flux at the moving boundary $b(t)$. At the moving boundary $x = b(t)$ using Glen's flow law and the assumption of unidirectional flow the diffusive velocity u satisfies [11]

$$\left. \frac{\partial u}{\partial x} \right|_{b(t)} = A \left[\frac{1}{4} \rho_i g \left(1 - \frac{\rho_i}{\rho_w} \right)^n \right] h^n \quad (2)$$

where $h = h(b(t))$ and A is a constant known as the rate factor and is taken from Glen's flow law. Although the rate factor is dependent on the temperature of the ice (and in practice has a large impact in the speed of the ice flow), for the simplified model used in this dissertation we have taken it to be constant, its value being chosen as the value used in the EISMINT suite of test problems [11].

As the diffusive velocity $u(x, t)$ behaves very differently in the sheet and the shelf we split the problem into two sub-problems. Let $a(t)$ be the time dependent position of the grounding line, where $0 \leq a(t) \leq b(t)$. Then $x \in [0, a(t)]$ is the ice sheet region and $x \in [a(t), b(t)]$ is the ice shelf region.

1.3.1 The Ice Sheet

Using the physics of ice in the ice sheet region $0 \leq x \leq a(t)$ the vertically averaged diffusive velocity u is given in [11] as

$$u = -C \left(\frac{\partial s}{\partial x} \right)^n h^{n+1} \quad (3)$$

where n is the flow law exponent in Glen's flow law (generally accepted to be $n = 3$), and s is the surface elevation which is the sum of the ice thickness and any elevation of the bed rock. As we are assuming that the bed is flat we can allow s to be equal to the ice thickness h . In equation (3) C is a constant given by

$$C = \frac{2A(\rho_i g)^3}{5}$$

Note that we can rewrite the diffusive velocity (3) in the ice sheet as

$$u = -C \left(\frac{\partial h}{\partial x} \right)^3 h^4. \quad (4)$$

for use in the mass balance equation (1).

1.3.2 The Ice Shelf

In the ice shelf region $a(t) \leq x \leq b(t)$ the diffusive velocity is defined differently by the elliptic equation [11]

$$2 \frac{\partial}{\partial x} \left[\nu h \frac{\partial u}{\partial x} \right] = \rho g h \frac{\partial s}{\partial x} \quad (5)$$

where ν is the viscosity. It is necessary to solve the differential equation (5) for u for use in the mass balance equation (1).

To find the surface elevation of the ice shelf we must again make use of the flotation criterion. Let $(l - b)$ be the difference between the sea level and the ice base elevation. Computing this value for the ice shelf will give us the depth of the bottom ice surface below sea level, which we call h' . We can then compute the surface elevation using

$$s = l + (h - h').$$

In figure 2 these features have been added to figure 1 for clarity. To recover the depth of the ice shelf base we must again make use of the flotation criterion. As $l - b$ is the difference between sea level and the elevation of the ice base, this will give us the thickness of the ice under the sea level. Therefore $l - \frac{\rho_i}{\rho_w} h$ will give the elevation of the ice base.

We can also use the the flotation criterion to find the sea level. We expect the

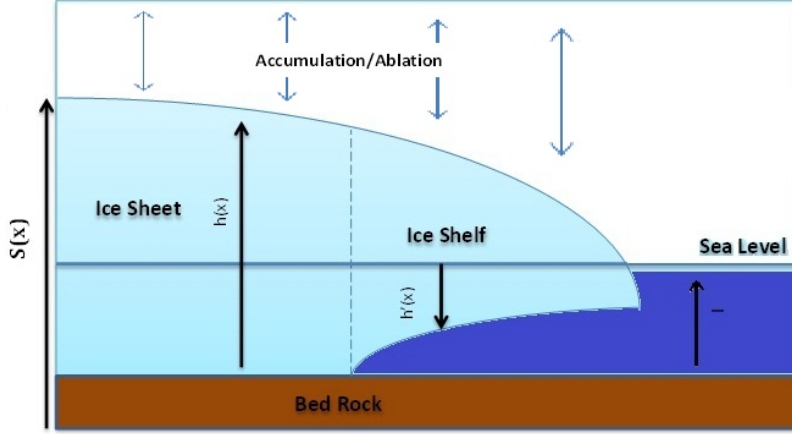


Figure 2: Illustration of Glacier

thickness of the ice below sea level to be equal to the sea level at the grounding line and so

$$l - \frac{\rho_i}{\rho_w} h_a = 0$$

where h_a is the the ice thickness at the grounding line. We can then calculate sea level by

$$l = \frac{\rho_i}{\rho_w} h_a.$$

In this work we shall assume that the sea level is constant over time and space. Note that in both the sheet and the shelf u depends on h and h_x so that equation (1) is a nonlinear diffusion equation with a moving boundary.

1.3.3 Interface Condition

The interface conditions at the grounding line $a(t)$ are that h and h_x are continuous (which implies that the flux is continuous). There is also a migration rate at the grounding line. In order to find the migration rate a new equation is introduced. The flotation condition stated earlier is

$$\rho_i h = \rho_w (l - b).$$

From a total differentiation of the flotation condition, the grounding line migration rate is given in [11] by

$$\frac{da}{dt} = \frac{\frac{\rho_w}{\rho_i} \frac{\partial f}{\partial t} + \frac{\partial(hu)}{\partial x} - m}{\frac{\partial h}{\partial x} - \frac{\rho_w}{\rho_i} \frac{\partial f}{\partial x}} \quad (6)$$

where $f = (l - h)$ is defined as the water depth at the grounding line and m is the accumulation rate.

The position of the grounding line is dependent on the local conditions and will

advance or recede depending on the changes of mass in the ice sheet and shelf. As we are assuming that sea level remains constant, then the position of the grounding line depends only on the thickness of the ice sheet at the grounding line. If the rate of accumulation in the sheet is greater than the combination of ablation and ice diffusing into the shelf then we would expect the mass to increase and the ice to thicken. If the ice thickens we would need more water to support the weight of the ice and as we are assuming that the sea level remains constant then the position of the grounding line will advance. In contrast, if there is a higher rate of ablation and diffusion from the sheet than accumulation to the sheet we expect to see the mass decrease and so the ice thickness will decrease and the grounding line will recede.

1.3.4 Total Mass Balance

We define the total mass of the ice in the sheet and shelf together as:

$$\theta = \int_0^{b(t)} h(x, t) dx.$$

Since it has been assumed that there is no flux out of the system at $x = 0$ and so $hu = 0$, we can show using Leibnitz integral rule that

$$\begin{aligned} \dot{\theta} = \frac{d}{dt} \int_0^{b(t)} h dx &= \int_0^{b(t)} h_t dx + h \frac{db}{dt} \Big|_{x=b(t)} \\ &= \int_0^{b(t)} -(hu)_x dx + \int_0^{b(t)} m dx + h \frac{db}{dt} \Big|_{x=b(t)} \\ &= \int_0^{b(t)} m dx + \left(-hu + h \frac{db}{dt} \right) \Big|_{x=b(t)} \\ &= \int_0^{b(t)} m dx \end{aligned} \tag{7}$$

since $u = \frac{db}{dt}$ at $x = b(t)$. This implies that the change in mass is entirely dependent on the accumulation term m . The rate of change is equal to the total amount of accumulation or ablation over the whole glacier.

1.4 Outline of the Dissertation

The main aims of this dissertation are to

1. Investigate the efficiency of a moving mesh scheme based upon conserving mass fractions in modelling the migration of the grounding line.
2. Investigate the behaviour of the approximate glacier dynamics of this scheme

In section 2 we investigate the behaviour of the diffusive velocity u in the sheet and shelf separately without the accumulation term m . We go on to discuss the numerical approximations used for both the sheet and shelf in section 2.3.

We then combine in section 3 the sheet and shelf calculations and the coupling between them. At this point an approach using conservation of mass fractions (CMF) is introduced. The mass fractions induce a deformation velocity v , which is generated by the diffusive velocity u and the coupling between the sheet and the shelf. This deformation velocity is then used to move the mesh. We are then able to recover the ice thickness algebraically using the local conservation principle. As this approach cannot be carried through analytically we need to find feasible ways to do it numerically. The numerical approximations for the deformation velocities and the recovery of the ice height using finite differences are also given in section 3. In section 4 we add the source term and outline the effect this has on the basic theory including the numerical algorithm.

In section 5 we discuss the non-dimensionalisation of the equations. In section 6 we use a test problem to investigate the significance of the viscosity of the ice and discuss a steady state solution. We go on to demonstrate the convergence of the moving mesh method used in this dissertation. We then go on to talk about the sensitivity of the model to various rates of accumulation in section 7.

In section 8 we introduce an elevation to the glacier bed. We discuss how this affects the model and also how the stability of the method is affected with varying gradients in the elevation. In section 9 we discuss the influence that changes in sea level has on the grounding line and finally in section 10 we investigate the influence that the rate factor A has on the evolution of the glacier.

Throughout sections 7 to 10 we compare results where appropriate, with the EISMINT test cases and the results in the Vieli and Payne survey paper [11].

To conclude we give a brief summary of our findings and discuss further work on improvements and generalisations.

2 Ice Diffusion Only

In this section we consider the problem with the accumulation term m set to zero. Equation (1) then becomes the simpler equation:

$$h_t = -(hu)_x. \quad (8)$$

Previously from equation (7) we showed that the change in mass is equal to the net accumulation. As we are now disregarding the accumulation term we can now say that

$$\dot{\theta} = \frac{d}{dt} \int_0^{b(t)} h dx = 0$$

and so

$$\int_0^{b(t)} h dx = \text{Constant}.$$

2.1 Ice Sheet

The ice sheet covers the region $0 \leq x \leq a(t)$. The boundary conditions for the ice sheet alone are that $\frac{\partial h}{\partial x} = 0$ and there is zero flux at the fixed boundary $x = 0$ and that there is no flux out the moving boundary $a(t)$ where $\frac{\partial h}{\partial x}$ and $u(a(t))$ is given. The diffusive velocity is given in equation (4) and remains the same for a system without accumulation.

If we substitute u from equation (4) into equation (8) we obtain the following nonlinear diffusion equation for h :

$$h_t = C \left(h^5 \left(\frac{\partial h}{\partial x} \right)^3 \right)_x \quad (9)$$

We can also make use of the fact that $h_x^3 h^4 = \left(\frac{3}{7}\right)^3 (h^{7/3})_x^3$ to rewrite the formula for u as

$$u = -c [(h^{7/3})_x]^3 \quad (10)$$

where

$$c = C \left(\frac{3}{7} \right)^3$$

leading to the alternative form of the nonlinear equation (9)

$$h_t = c \left(h \left(\frac{\partial h^{7/3}}{\partial x} \right)^3 \right)_x \quad (11)$$

for the change in thickness h in the ice sheet. It is equation (11) we have to solve for h in $(0, a(t))$ subject to the given boundary conditions.

2.2 Ice Shelf

The ice shelf covers the region $a(t) \leq x \leq b(t)$; the absence of accumulation does not affect the equation for u given in equation (5), so u must satisfy the differential equation

$$2 \frac{\partial}{\partial x} \left[\nu h \frac{\partial u}{\partial x} \right] = \rho g h \frac{\partial s}{\partial x} \quad (12)$$

We consider two scenarios for the shelf velocity, one where the viscosity ν is constant, and a more realistic model for a variable viscosity defined by [11]

$$\nu = A^{-1/3} \left(\frac{\partial u}{\partial x} \right)^{-2/3}. \quad (13)$$

In the constant viscosity case u is given by equation (12) which is a linear elliptic equation. Incorporating the variable viscosity in equation (13) into the elliptic equation (12), the ice shelf diffusive velocity u must now satisfy

$$\begin{aligned} 2 \frac{\partial}{\partial x} \left[h A^{-1/3} \left(\frac{\partial u}{\partial x} \right)^{-2/3} \frac{\partial u}{\partial x} \right] &= \rho g h \frac{\partial s}{\partial x} \\ \implies 2 \frac{\partial}{\partial x} \left[h \left(\frac{\partial u}{\partial x} \right)^{\frac{1}{3}} \right] &= A^{1/3} \rho g h \frac{\partial s}{\partial x}. \end{aligned} \quad (14)$$

This is a non-linear elliptic equation.

The boundary conditions at $b(t)$ have been stated earlier in equation (2). In this separate model we also assume that when the shelf is modelled by itself we are given the diffusive velocity u at $x = a(t)$.

2.3 Numerical Approximations

In order to solve the differential equations for this problem we turn to numerical methods to approximate the solution. As mentioned in the introduction we use

a moving mesh model. One of the ideas behind a moving mesh grid is to allow the grounding line to be followed continuously [11]. This approach is considered advantageous from a numerical point of view since the grounding line is part of the solution and no interpolation is needed [5]. Fixed grid models generally employ some interpolation, as the grounding line could be situated between two fixed grid points. In the survey paper of Vieli and Payne [11] it was found that fixed grid models are more dependent on numerical details such as grid size and so are not as robust as moving grid models [11]. The numerical scheme used in this dissertation adopts one particular moving mesh approach, which incorporates conserved mass fractions to move the mesh.

The domain $[0, b(t)]$ is divided into N intervals such that the initial spacing is constant, i.e. $\Delta x = b(0)/N$. As we are dealing with two separate domains we will use a subscript 1 to denote the sheet and 2 for the shelf (e.g. N_1 for the sheet and N_2 for the shelf, where $N_1 + N_2 = N$). We will initially take equal intervals $\Delta x_1 = a(0)/N_1$ for the ice sheet and $\Delta x_2 = (b(0) - a(0))/N_2$ for the ice shelf, such that $x(j) = j\Delta x_1$ for $j = (0, \dots, N_1)$ is the distance along the ice sheet and $x(j) = j\Delta x_2$ for $j = (N_1, \dots, N_2)$ is the distance along the ice shelf. Subsequently the intervals Δx_1 and Δx_2 will vary with time.

The diffusive velocity is approximated using finite difference schemes.

2.3.1 Ice Sheet

For the ice sheet a centred finite difference scheme is used at the interior points,

$$u_j = c \left(\frac{(h_{j+1})^{7/3} - (h_{j-1})^{7/3}}{x_{j+1} - x_{j-1}} \right)^3. \quad (15)$$

for $j = 1, \dots, N_1 - 1$. At $j = 0$ we use the fact that $\frac{dh}{dx} = 0$ and so $h_1 = h_{-1}$ which implies that $u_0 = 0$. At the boundary $x = a(t)$ a downwind scheme is used..

2.3.2 Ice Shelf

For the ice shelf we have two different approximations, firstly the approximation for a constant ν which gives us the linear elliptic equation given in (12) to solve, and secondly the approximation for a varying viscosity which gives the non-linear elliptic equation given in equation (14).

We approximate equation (12) using centred differences as follows:

$$\frac{2h_{j+1/2} \left(\frac{u_{j+1} - u_j}{x_{j+1} - x_j} \right) - 2h_{j-1/2} \left(\frac{u_j - u_{j-1}}{x_j - x_{j-1}} \right)}{x_{j+1/2} - x_{j-1/2}} = \nu^{-1} \rho g h_j \frac{s_{j+1/2} - s_{j-1/2}}{x_{j+1/2} - x_{j-1/2}} \quad (16)$$

$j = N_1 + 1, \dots, N_2 - 1$. We use the midpoint average for half values h and s to get

$$(h_{j+1} + h_j) \left(\frac{u_{j+1} - u_j}{x_{j+1} - x_j} \right) - (h_j + h_{j-1}) \left(\frac{u_j - u_{j-1}}{x_j - x_{j-1}} \right) = \nu^{-1} \rho g h_j \frac{s_{j+1} - s_{j-1}}{2} \quad (17)$$

and so

$$\frac{h_j + h_{j-1}}{x_j - x_{j-1}} u_{j-1} - \left(\frac{h_{j+1} + h_j}{x_{j+1} - x_j} + \frac{h_j + h_{j-1}}{x_j - x_{j-1}} \right) u_j + \frac{h_{j+1} + h_j}{x_{j+1} - x_j} u_{j+1} = \nu^{-1} \rho g h_j \frac{s_{j+1} - s_{j-1}}{2} \quad (18)$$

This can be written as a system of linear equations.

At the boundary $j = N_1$, u_0 is given. For the boundary at $x = b$ instead of a centred difference approximation we use a backward difference approximation

$$2h_j \left(\frac{\partial u}{\partial x} \right)_N - 2(h_N + h_{N-1}) \left(\frac{u_N - u_{N-1}}{x_N - x_{N-1}} \right) = \nu^{-1} \rho g h_N \frac{s_N - s_{N-1}}{2} \quad (19)$$

and use the boundary condition given in equation (2).

Thus the system of equation is given as

$$\begin{pmatrix} \left(\frac{h_2+h_1}{x_2-x_1} + \frac{h_1+h_0}{x_1-x_0} \right) & \frac{h_2+h_1}{x_2-x_1} & \dots & 0 \\ \frac{h_2+h_1}{x_2-x_1} & - \left(\frac{h_3+h_2}{x_3-x_2} + \frac{h_2+h_1}{x_2-x_1} \right) & \frac{h_3+h_2}{x_3-x_2} & 0 \\ \vdots & \ddots & \ddots & \vdots \\ \vdots & \ddots & \ddots & \vdots \\ \vdots & \ddots & \ddots & \vdots \\ \vdots & \frac{h_{N-1}+h_{N-2}}{x_{N-1}-x_{N-2}} & - \left(\frac{h_N+h_{N-1}}{x_N-x_{N-1}} + \frac{h_{N-1}+h_{N-2}}{x_{N-1}-x_{N-2}} \right) & \frac{h_N+h_{N-1}}{x_N-x_{N-1}} \\ 0 & 0 & \frac{h_N+h_{N-1}}{x_N-x_{N-1}} & \frac{h_N+h_{N-1}}{x_N-x_{N-1}} \end{pmatrix} \begin{pmatrix} u_1 \\ u_2 \\ \vdots \\ \vdots \\ \vdots \\ \vdots \\ u_N \end{pmatrix} = \begin{pmatrix} \nu^{-1} \rho g h_1 \frac{s_2-s_0}{2} - \frac{h_1+h_0}{x_1-x_0} u_0 \\ \nu^{-1} \rho g h_2 \frac{s_3-s_1}{2} \\ \vdots \\ \vdots \\ \vdots \\ \nu^{-1} \rho g h_N \frac{s_N-s_{N-1}}{2} - 2A \left(\frac{1}{4} \rho_i g \left(1 - \frac{\rho_i}{\rho_w} \right) \right)^3 h_N^4 \end{pmatrix} \quad (20)$$

This is a tridiagonal system which we can solve for the diffusive shelf velocities u using Gaussian elimination.

For the non-linear elliptic equation with varying viscosity we employ a different method to approximate the diffusive velocity u . For this we will use Picard iteration. This is a simple first order iteration method. Given the equation

$$2 \frac{\partial}{\partial x} \left[h \left(\frac{\partial u}{\partial x} \right)^{1/3} \right] = A^{1/3} \rho g h \frac{\partial s}{\partial x}$$

from section 2.2, a finite difference scheme will give us the following approximation

$$\frac{2h_{j+1/2} \left(\frac{u_{j+1} - u_j}{x_{j+1} - x_j} \right)^{1/3} - 2h_{j-1/2} \left(\frac{u_j - u_{j-1}}{x_j - x_{j-1}} \right)^{1/3}}{x_{j+1/2} - x_{j-1/2}} = A^{1/3} \rho g h_j \frac{s_{j+1/2} - s_{j-1/2}}{x_{j+1/2} - x_{j-1/2}} \quad (21)$$

We are able to use the midpoint average for half values h and s to get

$$(h_{j+1} + h_j) \left(\frac{u_{j+1} - u_j}{x_{j+1} - x_j} \right)^{1/3} - (h_j + h_{j-1}) \left(\frac{u_j - u_{j-1}}{x_j - x_{j-1}} \right)^{1/3} = A^{1/3} \rho g h_j \frac{s_{j+1} - s_{j-1}}{2} \quad (22)$$

So u_j satisfies the nonlinear system

$$(h_{j+1} + h_j) \left(\frac{u_{j+1} - u_j}{x_{j+1} - x_j} \right)^{1/3} - (h_j + h_{j-1}) \left(\frac{u_j - u_{j-1}}{x_j - x_{j-1}} \right)^{1/3} - A^{1/3} \rho g h_j \frac{s_{j+1} - s_{j-1}}{2} = 0 \quad (23)$$

for $j = N_1 + 1, \dots, N_2 - 1$.

For the boundary at $j = N_2$ instead of a centred difference approximation we will use a backwards difference approximation

$$h_j \left(\frac{\partial u}{\partial x} \right)_b^{1/3} - (h_j + h_{j-1}) \left(\frac{u_j - u_{j-1}}{x_j - x_{j-1}} \right)^{1/3} - A^{1/3} \rho g h_j \frac{s_{j+1} - s_{j-1}}{2} = 0 \quad (24)$$

and apply the boundary condition described in equation (2). At $x = a(t)$ we will also use the given diffusive velocity u . We now have the following system of non linear equations

$$\mathbf{F}(\mathbf{u}) = \begin{pmatrix} (h_2 + h_1) \left(\frac{u_2 - u_1}{x_2 - x_1} \right)^{1/3} - (h_2 + h_a) \left(\frac{u_1 - u_a}{x_1 - x_a} \right)^{1/3} - A^{1/3} \rho g h_1 \frac{s_2 - s_a}{2} \\ (h_3 + h_2) \left(\frac{u_3 - u_2}{x_3 - x_2} \right)^{1/3} - (h_2 + h_1) \left(\frac{u_2 - u_1}{x_2 - x_1} \right)^{1/3} - A^{1/3} \rho g h_2 \frac{s_3 - s_1}{2} \\ \vdots \\ \vdots \\ \vdots \\ \vdots \\ \vdots \\ \vdots \\ \frac{h_j^2 A^{1/3} \rho g (1 - \frac{\rho_i}{\rho_w})}{4} - (h_N + h_{N-1}) \left(\frac{u_N - u_{N-1}}{x_N - x_{N-1}} \right)^{1/3} - A^{1/3} \rho g h_N \frac{s_N - s_{N-1}}{2} \end{pmatrix} = \mathbf{0} \quad (25)$$

Taking an initial guess for the diffusive velocity and using the Picard iterative

method,

$$\mathbf{u}^{new} = \mathbf{u}^{old} - \mathbf{F}(\mathbf{u}^{old})$$

we can find the diffusive velocity of the ice shelf provided that the iterations converge. This will only happen if the iteration is a contraction and in order to achieve this we will use a relaxation coefficient $\phi = 0.01$ such that

$$\mathbf{u}^{new} = \mathbf{u}^{old} - \phi \mathbf{F}(\mathbf{u}^{old}).$$

2.3.3 Advancement of x and Recovery of h

Once we have calculated the approximate velocities for each point in the sheet and shelf we can move each grid point with the calculated velocity using the explicit Euler method

$$x_j^{n+1} = x_j^n + \Delta t u_j^n \quad (26)$$

where Δt is a chosen time step and the superfix denotes the time level.

It is now possible to recover the new values of h using Leibnitz Rule and equation (8)

$$\frac{d}{dt} \int h dx = \int \left[\frac{\partial h}{\partial t} + (hu)_x \right] dx = 0$$

for arbitrary limits, we have

$$\int_{x_{j-1}}^{x_{j+1}} h dx = c_j \quad (27)$$

where c_i is a mass constant. The integral is approximated by a midpoint rule, leading to

$$h_j(x_{j+1} - x_{j-1}) = c_j \quad (28)$$

These mass constants can be calculated for each subinterval using the initial conditions. i.e.

$$c_j = h_j^0(x_{j+1}^0 - x_{j-1}^0) \quad (29)$$

where the superfix 0 represents the values at the initial time. As the mass constants stay constant over time the ice thickness can be recovered using the approximation of the conservation principle (28) after the gridpoints have been moved. We do this using the following midpoint approximation and rearrangement of equation (28),

$$h_j = \frac{c_j}{x_{j+1} - x_{j-1}}. \quad (30)$$

A key factor in the moving mesh method we apply in this dissertation is that we allow local mass fractions to be preserved in the moving mesh. The significance of this is that the method is locally mass conserving when $m = 0$. This is in contrast to other

moving mesh methods where a purely geometrical criterion is often employed. In such methods the moving domain $x \in [0, b(t)]$ is mapped to a fixed domain $\xi \in [0, 1]$ by the transformation $\xi = \frac{x}{b(t)}, \tau = t$. Using the chain rule to differentiate $h(\xi, \tau)$ with respect to τ and ξ transforms (1) into

$$\frac{\partial h}{\partial t} - \frac{\xi}{b(\tau)} \frac{\partial b(\tau)}{\partial \tau} + \frac{\partial(hu)}{\partial \xi} = m \quad (31)$$

Note that this approach adds another term to the left hand side that is not a total derivative with respect to ξ and therefore the equation is no longer in divergent form. This feature can lead to unphysical effects in the method, such as not being mass conserving when $m = 0$.

3 Combining the Ice Sheet and Ice Shelf

To combine the ice sheet and ice shelf we must replace the boundary conditions at $a(t)$ by the interface condition introduced in section 1.3.3. As we are disregarding the accumulation term in this section we put $m = 0$ and so the total mass of the system is constant. This simplification allows us to rewrite the grounding line migration rate given in equation (6), which we will now refer to as v_a , as:

$$v_a = \frac{da}{dt} = \frac{\frac{\rho_w}{\rho_i} \frac{\partial f}{\partial t} + \frac{\partial(hu)}{\partial x}}{\frac{\partial h}{\partial x} - \frac{\rho_w}{\rho_i} \frac{\partial f}{\partial x}} \quad (32)$$

If we were to combine the ice sheet and ice shelf so that we were simply calculating the values for the ice sheet and the ice shelf separately in the same time step we would not admit coupling between the two. This is not the case as there is an interchange of flux between the ice sheet and ice shelf. The result is that although the total mass in the system will remain constant, the masses in each section will not, so the constants c_j in section 2.3.3 will need adjusting.

3.1 Mass Fractions

We now define the ice masses in the sheet and shelf as

$$\theta_1 = \int_0^{a(t)} h_1 dx, \quad \theta_2 = \int_{a(t)}^{b(t)} h_2 dx,$$

where h_1 and h_2 are the heights for the sheet and shelf respectively. As before the total mass is

$$\theta = \theta_1 + \theta_2 = \int_0^{b(t)} h dx$$

which is constant and where $\theta_1, \theta_2 \neq 0$ and so differentiating with respect to time gives

$$\frac{d\theta}{dt} = \dot{\theta} = \dot{\theta}_1 + \dot{\theta}_2 = 0. \quad (33)$$

We now introduce mass fractions c_1 and c_2 , defined as:

$$\frac{1}{\theta_1} \int_0^{x(t)} h_1 dx = c_1(0, x), \quad \frac{1}{\theta_2} \int_{x(t)}^{b(t)} h_2 dx = c_2(x, b). \quad (34)$$

Therefore both sheet and shelf are non-mass conserving problems although the entire

system is one. Observe that $c_1(0, a) = 1$ and $c_2(a, b) = 1$. When held constant these mass ratios can be used to induce modified velocities.

3.2 Deformation Velocities

We shall move the points $x(t)$ such that the mass fractions in equation (34) will remain constant over time, which we can do even with a non-zero flux between the ice sheet and shelf.

Whereas in equation (27) we could have written $\int_0^{x(t)} h_1(x, t) dx = c(0, x)$, we now have, from equation (34), that $\int_0^{x(t)} h_1 dx = \theta_1 c(0, x)$ and so

$$\frac{d}{dt} \int_0^{x(t)} h_1 dx = \dot{\theta}_1 c_1(0, x) \quad (35)$$

and similarly

$$\frac{d}{dt} \int_{x(t)}^{b(t)} h_2 dx = \dot{\theta}_2 c_2(x, b). \quad (36)$$

Using Leibnitz Rule, we find that

$$\frac{d}{dt} \int_0^{x(t)} h_1 dx = \int_0^{x(t)} \frac{\partial h_1}{\partial t} dx + [hv]_0^{x(t)} \quad (37)$$

where $v = \frac{dx}{dt}$ is the modified velocity which is induced by the mass fractions. We can substitute for $\frac{\partial h_1}{\partial t}$ from the mass balance equation (8) to get

$$\begin{aligned} \frac{d}{dt} \int_0^{x(t)} h_1 dx &= \int_0^{x(t)} (-(h_1 u_1)_x + (h_1 v_1)_x) dx \\ &= [h_1(-u_1 + v_1)]_0^{x(t)} \\ &= h_1(x)(-u_1(x) + v_1(x)) \end{aligned} \quad (38)$$

since $v_1(0) = u_1(0) = 0$. Hence

$$h_1(x)(-u_1(x) + v_1(x)) = \dot{\theta}_1 c_1(0, x)$$

giving

$$v_1(x) = u_1(x) + \frac{\dot{\theta}_1 c_1(0, x)}{h_1(x)} \quad (39)$$

by equation (35).

Similarly

$$\begin{aligned}\frac{d}{dt} \int_{x(t)}^{b(t)} h_2 dx &= \int_{x(t)}^{b(t)} (-(h_2 u_2)_x + (h_2 v_2)_x) dx \\ &= [h_2(-u_2 + v_2)]_{x(t)}^{b(t)}\end{aligned}$$

$$\frac{d}{dt} \int_{x(t)}^{b(t)} h_2 dx = h_2(b)(-u_2(b) + v_2(b)) - h_2(x)(-u_2(x) + v_2(x)). \quad (40)$$

Hence

$$h_2(b)(-u_2(b) + v_2(b)) - h_2(x)(-u_2(x) + v_2(x)) = \dot{\theta}_2 c_2(x, b)$$

by equation (36). As we have zero flux at the boundary $x = b$, then $h_2(b)(-u_2(b) + v_2(b)) = 0$, $\forall h_2(b)$ and so $v_2(b) = u_2(b)$. Therefore

$$v_2(x) = u_2(x) - \frac{\dot{\theta}_2 c_2(x, b)}{h_2(x)}. \quad (41)$$

Putting $x = a$ into equations (39) and (41) gives us that $\dot{\theta}_1 = h_a(-u_a + v_a) = -\dot{\theta}_2$ as we expected from equation (33). Substituting this into equations (39) and (41) we get the deformation velocities

$$v_1(x) = u_1(x) + \frac{h_a}{h_1(x)} c_1(0, x)(-u_a + v_a) \quad (42)$$

$$v_2(x) = u_2(x) + \frac{h_a}{h_2(x)} c_2(x, b)(-u_a + v_a) \quad (43)$$

Note that

$$c(b, b) = \frac{1}{\theta_2} \int_{b(0)}^{b(0)} h_2 dx = 0$$

and so the addition to the diffusive velocity incurred by the deformation caused by the mass fractions is zero at the shelf front.

3.3 Numerical Approximations

First we approximate the grounding line migration rate v_a in equation (32) using a centred difference. Let $j = a$ be the position of $a(t)$ at a given time, then

$$v_a = \frac{\frac{\rho_w}{\rho_i} \frac{f^{new} - f^{old}}{\Delta t} + \frac{(hu)_{a+1} - (hu)_{a-1}}{x_{a+1} - x_{a-1}}}{\frac{h_{a+1} - h_{a-1}}{x_{a+1} - x_{a-1}} - \frac{\rho_w}{\rho_i} \frac{f_{a+1} - f_{a-1}}{x_{a+1} - x_{a-1}}}.$$

3.3.1 Time Stepping

Once we have the approximation v_a substituted into equations (42) and (43) we get the velocities of the moving points. We now move each grid point with its corresponding velocity, doing this in the same way as in section 3.3 equation (26). However instead of u_j , we now use v_j . Since θ_1 and θ_2 vary over time we must also find their new values after each time step. As in equation (26) these are calculated using the explicit Euler scheme as follows:

$$\theta_1^{n+1} = \theta_1^n + \Delta t \dot{\theta}_1, \quad \theta_2^{n+1} = \theta_2^n + \Delta t \dot{\theta}_2 \quad (44)$$

3.3.2 Recovering h

All that is left is to calculate the new ice heights. From equation (34) we can deduce that:

$$\frac{1}{\theta_1} \int_{x_{j-1}}^{x_{j+1}} h_1 dx = c_{1,j+1} - c_{1,j-1} \quad \text{and} \quad \frac{1}{\theta_2} \int_{x_{j-1}}^{x_{j+1}} h_2 dx = c_{2,j-1} - c_{2,j+1}$$

Note that for the ice shelf c_j gets smaller as we progress along the shelf and so we subtract c_{j+1} from c_{j-1} to achieve the same effect as for the ice sheet. Using the new values of θ_1 and θ_2 found in section 3.3.1 we find the new mass of ice between x_{j-1} and x_{j+1} by

$$\int_{x_{j-1}}^{x_{j+1}} h_1 dx = \theta_1 [c_{1,j+1} - c_{1,j-1}] \quad \text{and} \quad \int_{x_{j-1}}^{x_{j+1}} h_2 dx = \theta_2 [c_{2,j-1} - c_{2,j+1}] \quad (45)$$

Approximating the integrals by the midpoint rule again we can retrieve the new values for the ice heights as follows:

$$h_j = \frac{\theta_1 (c_{1,j+1} - c_{1,j-1})}{x_{j+1} - x_{j-1}}, \quad h_j = \frac{\theta_2 (c_{2,j-1} - c_{2,j+1})}{x_{j+1} - x_{j-1}} \quad (46)$$

A key benefit of our method having mass conserving local mass fractions is that we are able to recover the ice height using the local mass. This avoids using another equation to recover the ice height and therefore any additional error to build up.

3.3.3 Algorithm

For convenience, the algorithm has been summarised here:

1. Compute θ_1 and θ_2 in the initial profile by integrating h with respect to x between $(0, a(t))$ and $(a(t), b(t))$ respectively.

2. Calculate the mass fractions $c_1(0, x_j)$ for $j \in [0, \dots, N^1]$ and $c_2(x_j, b)$ for $j \in [N^1, \dots, N^2]$ by integrating h with respect to x between $(0, x_j)$ for $j \in [0, \dots, N^1]$ and $(x_j, b(t))$ $j \in [N^1, \dots, N^2]$ respectively.

Then at each time step

3. Calculate the deformation velocities using equations (42) and (43).
4. Move the grid nodes with the calculated velocities using the explicit Euler method.
5. Find the new values for θ_1 and θ_2 using the explicit Euler method.
6. Use the new values of θ_1 and θ_2 to find the new values of the mass fractions using equation (45).
7. Retrieve the new values of the ice height h_j from equation (46) using the mid-point rule and the new values of the mass fractions.

4 Adding the Source Term

Up until now we have only considered the problem where the accumulation is zero. This is unrealistic as we would usually expect either snow or melting to change the total mass. To incorporate this we will now reintroduce the accumulation term $m(x)$ back into the equations and investigate how this will affect the algorithm. The function m is independent of time and will initially be taken as a constant to simulate the conditions used in the Vielli and Payne survey paper [11].

The governing equation is now equation (1). Mass is no longer conserved but we may 'simply' generalise section 3. Substituting (1) into equation (37) gives

$$\frac{d}{dt} \int_0^{x(t)} h_1 dx = \int_0^{x(t)} -(hu)_x + m dx + [hv]_0^{x(t)} \quad (47)$$

which as in section 3 implies that

$$\dot{\theta}_1 c_1(0, x) = h_1(x)(-u_1(x) + v_1(x)) + \int_0^{x(t)} m dx. \quad (48)$$

Similarly,

$$\dot{\theta}_2 c_2(0, x) = -h_2(x)(-u_2(x) + v_2(x)) + \int_{x(t)}^{b(t)} m dx \quad (49)$$

In the same way as in section 3, we substitute $x = a(t)$ to find $\dot{\theta}_1$ and $\dot{\theta}_2$, giving

$$\dot{\theta}_1 = h_a(-u_a + v_a) + \int_0^a m dx \quad (50)$$

$$\dot{\theta}_2 = -h_a(-u_a + v_a) + \int_a^b m dx \quad (51)$$

Then, substituting equations (50) and (51) into equations (48) and (49),

$$(h_a(-u_a + v_a) + \int_0^{a(t)} m dx) c_1(0, x) = h_1(x)(-u_1(x) + v_1(x)) + \int_0^{x(t)} m dx \quad (52)$$

$$(-h_a(-u_a + v_a) + \int_{a(t)}^{b(t)} m dx) c_2(0, x) = -h_2(x)(-u_2(x) + v_2(x)) + \int_{x(t)}^{b(t)} m dx \quad (53)$$

so that rearranging gives

$$v_1(x) = u_1(x) + \frac{(h_a(-u_a + v_a) + \int_0^{a(t)} m dx)c_1(0, x) - \int_0^{x(t)} m dx}{h_1(x)} \quad (54)$$

$$v_2(x) = u_2(x) + \frac{(h_a(-u_a + v_a) - \int_{a(t)}^{b(t)} m dx)c_2(0, x) + \int_{x(t)}^{b(t)} m dx}{h_2(x)} \quad (55)$$

The grounding line migration rate is now the same as in equation 6 reproduced here for convenience,

$$v_a = \frac{\frac{\rho_w}{\rho_i} \frac{\partial f}{\partial t} + \frac{\partial(hu)}{\partial x}}{\frac{\partial h}{\partial x} - \frac{\rho_w}{\rho_i} \frac{\partial f}{\partial x}} - m(x).$$

Letting a denote the grid point for the grounding line we can approximate the migration rate by

$$v_a = \frac{\frac{\rho_w}{\rho_i} \frac{f^n - f^{n-1}}{\Delta t} + \frac{(hu)_{a+1} - (hu)_{a-1}}{x_{a+1} - x_{a-1}} - m_a}{\frac{h_{a+1} - a_{a-1}}{x_{a+1} - x_{a-1}} - \frac{\rho_w}{\rho_i} \frac{f_{a+1} - f_{a-1}}{x_{a+1} - x_{a-1}}}.$$

where the superfixes n and $n - 1$ represent the time levels.

Note that we update the grid points positions, θ_1 and θ_2 in the same way as in section 3 using the explicit Euler method in equations (26) and (44). All that is left is to recover the new ice heights from the mass constants as in equation (46). For convenience we will summarise the algorithm for the added accumulation term:

1. Compute θ_1 and θ_2 in the initial profile by integrating h with respect to x between $(0, a(t))$ and $(a(t), b(t))$ respectively.
2. Calculate the mass fractions $c_1(0, x_j)$ for $j \in [0, \dots, N^1]$ and $c_2(x_j, b)$ for $j \in [N^1, \dots, N^2]$ by integrating h with respect to x between $(0, x_j)$ for $j \in [0, \dots, N^1]$ and $(x_{j^2}, b(t))$ for $j \in [N^1, \dots, N^2]$ respectively.

For each time step:

3. Calculate the deformation velocities using equations (54) and (55).
4. Move the grid nodes with the calculated velocities using the explicit Euler method.
5. Find the new values for θ_1 and θ_2 using the explicit Euler method.
6. Use the new values of θ_1 and θ_2 to find the new values for the mass fractions using equation (45).
7. Retrieve the new values of the ice height h_j from equation (46) using the mid-point rule and the new mass fractions.

5 Non-Dimensionalisation

In order to compare with real data we proceed to make this model non-dimensional. Non-dimensionalisation is accomplished by dividing each variable by a constant scaling parameter. Suppose we scale h , u , x , t , and m so that

$$h^* = \frac{h}{[h]}, \quad x^* = \frac{x}{[x]}, \quad t^* = \frac{t}{[t]}, \quad u^* = \frac{u}{[u]}, \quad m^* = \frac{m}{[m]}$$

where the square brackets indicate the corresponding scaling parameter and the superfix $*$ represents the scaled variable.

From equation (1) we find that the scaled shallow ice equation becomes

$$\frac{[h]}{[t]} h_{x^*}^x + \frac{[h]}{[x]} [u] (h^* u^*)_{x^*} = [m] m^*.$$

For balance to be maintained within equation (1) we must have

$$\frac{[h]}{[t]} = \frac{[h]}{[x]} [u] = [m], \quad \text{so} \quad [t] = \frac{[x]}{[u]}, \quad \text{and} \quad [m] = \frac{[h]}{[x]} [u]$$

5.1 Sheet

Using the diffusive velocity equation for the sheet given in section 2.1 as

$$u = c \left(\frac{\partial h^{7/3}}{\partial x} \right)^3$$

we obtain the scaled ice diffusion velocity u^*

$$[u] u^* = -[c] \frac{[h]^7}{[x]^3} c^* \left[\frac{\partial (h^*)^{7/3}}{\partial x^*} \right]^3$$

where

$$c^* = \frac{c}{[c]}$$

Again we must ensure that both sides are balanced and so

$$[u] = [c] \frac{[h]^7}{[x]^3}$$

5.2 Shelf

In the shelf we have a differential equation for ice diffusion velocity repeated here for convenience,

$$-2(\nu h u_x)_x = \rho g h s_x.$$

In the case where ν is variable, given as $\nu = A^{-1/3}(u_x)^{-2/3}$, the diffusive velocity in the ice shelf satisfies

$$-2(h(u_x)^{1/3})_x = A^{1/3} \rho g h(s_x). \quad (56)$$

The constant c used in the sheet calculations is given by

$$c = \left(\frac{3}{7}\right)^3 \frac{2A\rho^3 g^3}{5}$$

Using this in equation (56) gives

$$-2(h(u_x)^{1/3})_x = \left(\left(\frac{7}{3}\right)^3 \frac{5c}{2}\right)^{1/3} h s_x.$$

Therefore the scaled expression for the shelf velocity is given by

$$-2 \frac{[h]}{[x]} \left(\frac{[u]}{[x]}\right)^{1/3} \frac{h^*(u_{x^*})^{1/3}}{\partial x^*} = [c]^{1/3} [h] \frac{[s]}{[x]} \left(\left(\frac{7}{3}\right)^3 \frac{5C^*}{2}\right)^{1/3} h^* \left(\frac{\partial s^*}{\partial x^*}\right).$$

For balance we need

$$\frac{[h]}{[x]} \left(\frac{[u]}{[x]}\right)^{1/3} = [c]^{1/3} \frac{[h]^2}{[x]}$$

and so $[u] = [c][x][h]^3$.

It is sufficient to choose two of the scaling parameters $[x]$ and $[t]$ say, and we will then be able to get the scaling parameters for the rest of the variables. The scaling parameters are kept separate for the ice sheet and shelf.

6 A 1D Test Case

Following the EISMINT test case [11] we consider a glacier where both the ice sheet and ice shelf have an initial length of $50km$. We also need an initial profile for the ice thickness; this has been chosen to be

$$h = (1 - 0.75x^2)^{3/7}, \quad x \in (0, 1) \quad (57)$$

which is similar to the initial profile chosen in [4]. Table 1 shows a summary of the parameters used in the model.

Value	Physical Parameter
$n = 3$	Flow Law Exponent
$A = 10^{-18}(Pa)^{-3}a^{-1}(*)$	Flow Law Parameter
$g = 9.81ms^{-1}$	Acceleration of Gravity
$\rho_i = 920kgm^{-3}$	Ice Density
$\rho_w = 1028kgm^{-3}$	Sea Water Density
(*) a stands for annum, which is equal to 1 year	

Table 1: Table of Parameters

6.1 Steady State

There is some debate about the possibility of glaciers achieving a steady state. It is the opinion of Weertman (1974) and Thomas and Bentley (1978) that only downward sloping beds can achieve stability with small perturbations. By contrast Hindmarsh (1996) suggests that 'neutral equilibrium' can be achieved on all basal slopes, that is the glacier can reach a new steady state close to the original after a perturbation of the grounding line.

First we must investigate if a steady state geometry is achievable for this model. The MISIMIP survey paper [5] defines an achieved steady state to be one at which the rate of change of the grounding line is $0.1ma^{-1}$, while the rate of change of thickness is $1ma^{-1}$. This would suggest that the defined steady state of the MISIMIP experiments is not an actual steady state where $h_t = 0$ but where h_t is sufficiently small.

For the Vieli and Payne paper [11] it was found that a steady state could occur for a moving mesh model with a constant non zero accumulation rate. For the method of this dissertation a steady state only occurs for a constant accumulation when m is sufficiently close to zero. This would indicate that the only steady state solution for this method is the arbitrary steady state when $(hu)_x \approx 0$.

Running the model with zero accumulation exhibits negligible change to the initial conditions, with the change to the grounding line position becoming less than $0.1ma^{-1}$ within 2 years. We might ask why the larger mass of the ice at the ice divide does not distribute itself along the domain over time. A glacier flows in the direction of decreasing surface elevation. As the shelf is buoyed by the ocean the surface elevation changes only marginally and so the flow is relatively small.

The inability of this model to reach a non-arbitrary steady state is worrying as this is significantly different to the results found in previous studies. The potential cause of this inability to reach steady state is choosing a constant accumulation across the glacier. Since the method conserves mass, a constant source term will not allow a steady state solution as there is no flux of mass out of the system. This implies that instead of the constant accumulation term given in the Vieli and Payne [11] paper it is better to represent the accumulation with a linear equation. We will let

$$\gamma(1 - \beta x)$$

represent the accumulation profile, where γ is a parameter used to control the scale of the accumulation and β determines where the source term changes from accumulation to ablation. If we choose γ and β such that

$$\int_0^{b(t)} m dx = 0.3ma^{-1}$$

then we find the initial ice profile meets the requirements of a steady state described in the MISMIP [5] papers with negligible change to the initial conditions (i.e. the change in grounding line position is less than $0.1ma^{-1}$ and the change in ice thickness is less than $1ma^{-1}$).

6.2 Viscosity

We are interested in the effect of simplifying the model, so viscosity is left as a constant. We ran the model with $\int_0^{b(t)} m(x) dx = 0.5ma^{-1}$ for varying N for 5000 years. Note that for a net accumulation of $0.5ma^{-1}$ we have chosen $\gamma = 0.0002$ and $\beta = \frac{3}{2}$. The approximations set out in the equations (20) and (25) have been used, one in the case of constant viscosity and the other using varying viscosity. The results are displayed in table 2 and table 3, with the relative differences shown in table 4. The difference in grounding line position (GLP) between the the two methods is very small, although it becomes slightly larger with increased resolution. Also the change in shelf front position differs between the two methods, the shelf front receding with the varying viscosity and advancing with the constant viscosity,

although the difference decreases with an increased resolution.

N	Δt	GLP	Shelf Front	h at GLP
11	0.01	50.249357	100.0000008	914.502872
21	0.25	50.400903	100.0000007	915.532212
41	0.0625	50.429636	100.0000008	915.721627
81	0.015625	50.432728	100.0000008	915.740688

Table 2: Table of Values for Constant Viscosity

N	Δt	GLP (km)	Shelf Front (km)	h at GLP (m)
11	0.01	50.252652	99.998139	914.511045
21	0.25	50.404234	99.998295	915.539494
41	0.0625	50.433251	99.998381	915.728938
81	0.015625	50.436981	99.998427	915.748842

Table 3: Table of Values for Varying Viscosity

N	Δt	GLP	Shelf Front	h at GLP
11	0.01	0.0065575%	0.0018616%	0.0008936%
21	0.0025	0.0066089%	0.0017057%	0.0007952%
41	0.000625	0.0071676%	0.0016193%	0.0007983%
81	0.00015625	0.0084320%	0.0015739%	0.0008904%

Table 4: Table of Relative Differences between Varying and Constant Viscosity

Although the differences are very small, constant viscosity is regarded as too crude an assumption to make and, as incorporating the varying viscosity is relatively simple, all future experiments viscosity will be taken as the variable case,

$$\nu = A^{-1/3} \left(\frac{\partial u}{\partial x} \right)^{-2/3}.$$

6.3 Convergence

To decide if this numerical scheme is a useful tool in predicting the evolution of grounding lines we must show that the method is convergent. The position of the grounding line for a series of increasing values of N and a decreasing series of values of Δt has been recorded in table 5. To maintain stability Δt has been chosen such that $\Delta t \propto N^{-2}$. Variable viscosity has been included and the accumulation rate has been taken to be $\int_0^{b(t)} m(x) dx = 0.5m a^{-1}$. The final time has been set relatively low at 2500 years. This has been chosen because running the model for long time periods with a very fine resolution is computationally costly.

We now need to calculate the errors. As we do not have an exact solution or any comparable raw data the value for the grounding line position with the finest

N	Δt	Position of Grounding Line	Ice Height
11	0.01	50.014602	913.835880
21	0.25	50.178554	914.982169
41	0.0625	50.215269	915.234004
81	0.015625	50.222920	915.285344
161	0.00390625	50.224352	915.293350
321	0.0009765625	50.224840	915.293729

Table 5: Table of Values

numerical mesh is used to act as an exact solution. The resulting relative errors are recorded in table 6.

N	Δt	Relative Error	
		GL	Ice Height
11	0.01	0.4186%	0.1593%
21	0.0025	0.0922%	0.0340%
41	0.000625	0.0191%	0.0065%
81	0.00015625	0.0038%	0.0009%
161	0.00390625	0.0010%	0.00004%

Table 6: Table of Errors

The relative errors decrease as the resolution increases and so the scheme appears to converge to the "exact" solution with increasing number of meshpoints. Therefore we can conclude that the method is likely to be convergent.

It can be said that if the error $\|re\|_{N^{-1}} \leq C(N^{-1})^p$ where C is some constant and p is the order of the scheme. Then due to the doubling of the number of nodes

$$\frac{\|re\|_N}{\|re\|_{2N}} \leq \frac{C(N^{-1})^p}{C(N^{-1})^p} = 2^p$$

If C is independent of N then the constants will cancel and as $\log_2 2 = 1$, taking $\log_2 \frac{\|re\|_N}{\|re\|_{2N}}$ will give us the order p . The table of results for $\log_2 \frac{\|re\|_N}{\|re\|_{2N}}$ for varying values of h can be seen in table 7.

$\log_2 \left(\frac{\ re\ _N}{\ re\ _{2N}} \right)$	Order	
	GLP	h
$\log_2 \left(\frac{\ re\ _{11}}{\ re\ _{21}} \right)$	2.1834	2.2263
$\log_2 \left(\frac{\ re\ _{21}}{\ re\ _{41}} \right)$	2.2739	2.3831
$\log_2 \left(\frac{\ re\ _{41}}{\ re\ _{81}} \right)$	2.3179	2.8324
$\log_2 \left(\frac{\ re\ _{81}}{\ re\ _{161}} \right)$	1.9787	4.4919

Table 7: Table of Log Ratios

These results show that the method is approximately second order. This is much higher than expected as we use several first order numerical approximations. It is most likely the result of using the results with a fine mesh as the 'exact' solution. The last value in the table is particularly high as the the mesh resolutions for this

value are fine enough to closely resemble to the 'exact' solution, this would imply that this value is misleading.

6.4 Velocity

The velocity of each grid point for two accumulation profiles has been plotted in figure 3. The solid lines show the velocity for a positive net accumulation of $\int_0^{b(t)} m(x)dx = 0.5ma^{-1}$ and the dashed lines show the velocity for a negative net accumulation of $\int_0^{b(t)} m(x)dx = -0.5ma^{-1}$. The velocities have been extracted after running the model for 15000 years with $\Delta t = 0.0025$, and $N = 21$.

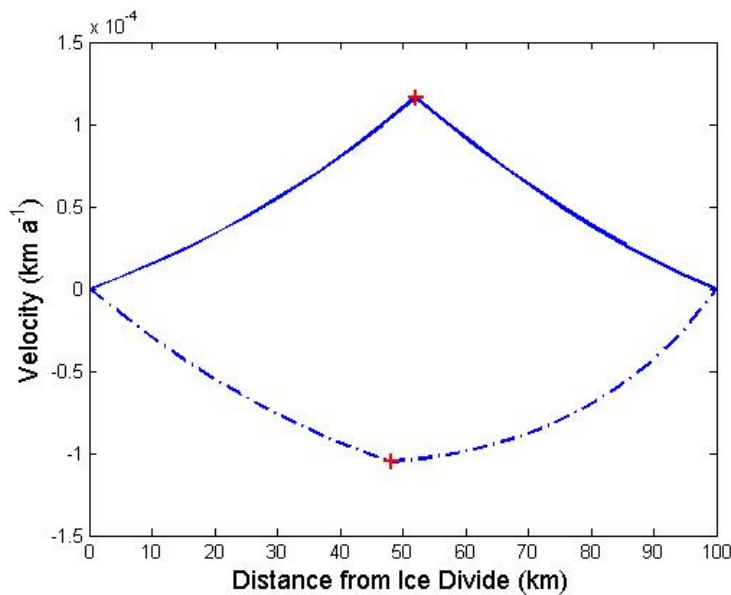


Figure 3: Velocity of Points of the Domain. The solid lines are for a positive net accumulation of $\int_0^{b(t)} m(x)dx = 0.5ma^{-1}$ and the dashed lines denote at negative net accumulation of $\int_0^{b(t)} m(x)dx = -0.5ma^{-1}$. The red crosses denote the grounding line position

For both accumulation rates the magnitudes of the velocities are much larger at the grounding line. This agrees with the results of Schoof [7].

6.5 Dependency on the Number of Nodes

From the Vieli and Payne paper [11], for the fixed grid models a step change in accumulation gives no change in grounding line position for a coarse grid. Increasing the resolution of the grid causes the grounding line to advance considerably if there is an increase in accumulation, however there is still no change to the grounding line position for a decrease in accumulation. This exhibits a strong dependency on grid

size and also a strong tendency for the grounding line to advance. In contrast to this there is no bias for the grounding line to advance or retreat for the moving mesh techniques of the Vieli and Payne paper. In addition, the difference in grounding line position between different numbers of grid nodes is much smaller for the moving mesh methods.

For our model there is some dependency of grounding line position on the number of grid points, however this is smaller than the initial Δx . Table 6 shows us that there is less than half a percent difference in grounding line position between a coarser grid and a finer grid, which amounts to approximately $200m$. This is less than the initial grid spacing and therefore in the resolution of the model. This shows us that the dependency on the number of grid points is small.

Table 5 shows that the change in grounding line position increases with increased N . This is contrary to the results of the Vieli and Payne survey paper [11]. Another difference between the moving mesh method of this dissertation and the ones used in the Vieli and Payne paper is that the tendency of the grounding line is dictated by the sign of the accumulation. For a positive net accumulation the grounding line will advance and for a negative accumulation the grounding line will recede. Whereas the grounding line in the Vieli and Payne paper models will recede for small positive values of accumulation.

To conclude, the moving mesh model used in this dissertation is less dependent on the number of nodes than the fixed grid models used in the Vieli and Payne paper and exhibits a similar dependency on the number of nodes to the moving mesh models of the Vieli and Payne paper.

6.6 Running Time of Model

The running time of the program to a final time of 10000 years has been given in table 8 to give an idea of how long the program takes to run.

N	Δt	Running Time (s)
11	0.01	0.173143
21	0.0025	0.73899
41	0.000625	3.626864
81	0.00015625	20.593795
161	0.0000390625	133.800593
321	0.000009765625	996.373773

Table 8: Table of Running Times

The computational cost of the program is relatively cheap with a running time of several minutes for a fine grid and a matter of seconds for a coarse grid.

7 Changes to the Accumulation Rate

For a positive net accumulation we expect the grounding line to advance and for a negative net accumulation we expect the grounding line to recede. For an increased magnitude in accumulation we would expect to see an increase in the change of grounding line position. The ice thickness profiles for different accumulation rates are shown in figure 4. Note that $\gamma = 0.0002$ and β is given various values with $\beta = \frac{3}{2}$ corresponding to a net accumulation of $0.5ma^{-1}$, $\beta = \frac{19}{10}$ corresponding to a net accumulation of $0.1ma^{-1}$, $\beta = \frac{21}{10}$ corresponding to a net accumulation of $-0.1ma^{-1}$ and $\beta = \frac{5}{2}$ corresponding to a net accumulation of $-0.5ma^{-1}$. The final time is $15ka$. There are 21 horizontal grid points for these plots and Δt has been taken to be 0.0025.

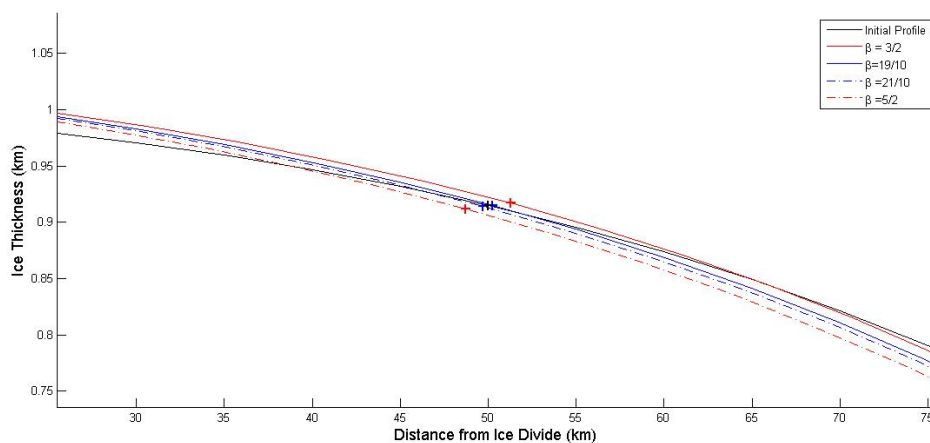


Figure 4: Ice thickness profile after 15000 years for different values of β . The crosses mark the grounding line position.

The expectations of the changes to the grounding line position with different accumulation rates have been met here. There is one key difference between the moving mesh method of this dissertation and those described in the Vieli and Payne survey paper. There are some cases in the Vieli and Payne paper that for even a positive accumulation there is still a retreat in the grounding line position. This is counter intuitive as a positive accumulation would indicate that there is mass gain. If the mass increases around the grounding line then it would require more water to buoy the mass of the ice. If the sea level remains constant then there will not be enough water to buoy the ice just ahead of the grounding line and so the flotation criterion will no longer be met. Thus the grounding line will advance. The fact that

this does not occur in the methods described in the Vieli and Payne survey paper [11] could be a symptom of mass not being relatively conserved.

We must now ask ourselves if the changes to grounding line position are reversible. This time we run the model with β changing during the model run. It starts with $\beta = \frac{3}{2}$, progresses to $\beta = \frac{19}{10}$ at $3750a$, $\beta = \frac{21}{10}$ at $7500a$, and finally $\beta = \frac{5}{2}$ at $11250a$. The grounding line position has been plotted against time with these changes to β in figure 5.

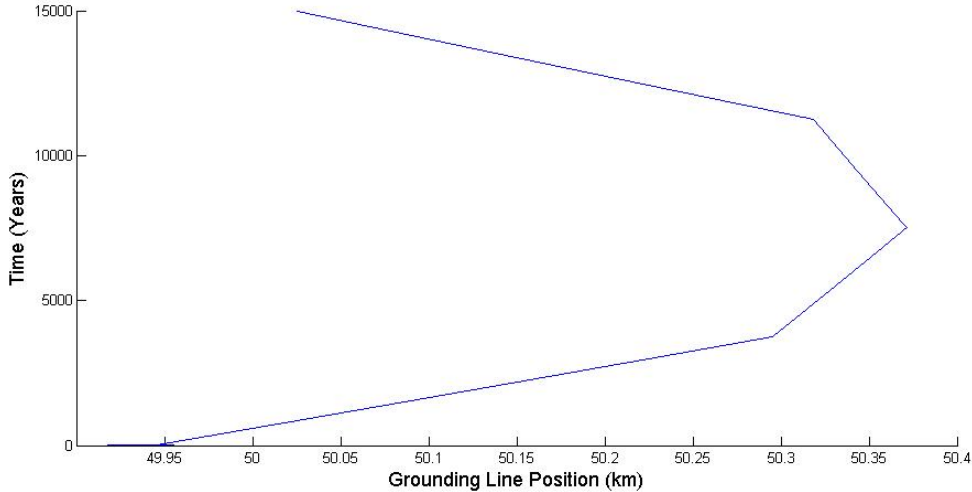


Figure 5: Change in grounding line position over 15000 years with β changing in time

Changes to the grounding line are clearly reversible, with the initial profile being achieved if the change of mass over a period of time equals the negative change of mass of the following period of time. From figure 5 we can also see that the grounding line position does not change more than $50m$ over $3750a$ when the net accumulation term is $0.1ma^{-1}$. The change in ice thickness is also less than $1ma^{-1}$. This would imply that under these conditions we are at an approximate steady state where h_t is sufficiently small. This would indicate that we have a 'neutral equilibrium', (i.e. there is a new steady state position close to the original).

The Vieli and Payne paper [11] saw that any change in the grounding line position can be reversed by resetting the accumulation term. The moving mesh method used here does not do this. This is because the accumulation term includes the net accumulation (i.e. accumulation + ablation) and as our method is locally mass conserving any change in mass is equal to the sum of accumulation over the glacier. Resetting the accumulation rate to what it was will only cause the grounding line to return to the original position if the original accumulation rate has the opposite sign to the new accumulation rate.

8 Introducing a Tilt

Up until now we have only discussed a glacier with a flat bed but in reality this is not the case. In order to make the model more realistic we now incorporate an elevation to the ice bed. This will change the way in which we treat the diffusive velocity set out earlier in equation (3). We previously stated that, in the sheet $s = h$ in the absence of bed elevation and so equation (3) could be adjusted to equation (10). As this is no longer the case we are left with equation (3) without any further simplification.

The bed elevation will also change the way we calculate sea level as we have a new component. As before we expect the sea level to be equal to the ice thickness below sea level at the grounding line. Hence

$$l = \frac{\rho_i}{\rho_w} h_a + b$$

where b is the elevation of the ice sheet base. At the grounding line this is equal to the elevation of the bed.

We choose three different profiles for the ice bed. An inclined plane with a slope of -0.005° with an elevation of $250m$ at the ice divide, an upward plane with a slope of 0.005° with an elevation of $250m$ at the shelf front and the previous bed rock profile of a flat bed. These have been chosen to replicate the EISMINT conditions [11]. The initial profiles of these glaciers are given in figure 6. All profiles have the same ice thickness profile, given in equation (57).

There is much debate as to whether it is possible for an upward sloping bed to be stable. Influential articles such as Weertman [12], and Thomas and Bentley [8], have led us to believe that stable marine ice sheets cannot be located on upward sloping beds. This instability can be explained by the ice sheet instability hypothesis, which states that if the grounding line recedes on an upward sloping bed then the thickness at the grounding line should increase. Ice flux in a one-dimensional model can be described by the equation $q = hu$, and so an increase in ice thickness leads to an increase in flux. As the flux increases as the grounding line recedes, then the grounding line will continue to recede indefinitely. This has been somewhat controversial, however. Hindmarsh [3] has argued that the large scale flow of the ice sheet is mostly unaffected by the changes to the grounding line position and that the ice sheet will therefore be stable on an upsloping bed [2]. Shoof [7] provides a combination of numerical and analytical results to confirm the work of Weertman [12] and Thomas and Bentley [8]. The survey paper of Vieli and Payne, [11] asserts

that the grounding line positions in moving mesh models are independent of basal slope. With such a varying field of conclusions and results it is still uncertain how the basal slope should affect the grounding line position.

We are interested in observing the impact of bed elevation on the migration of the grounding line for this moving mesh model. The model has been run for each glacier profile from figure 6 for a final time of 15000 years with $\int_0^{b(t)} m(x)dx = 0.5ma^{-1}$. and with $\int_0^{b(t)} m(x)dx = -0.5ma^{-1}$. There are 21 grid points, and $dt = 0.0025$. There is less than a $200m$ difference in grounding line position between the basal slopes for either an advance or a retreat. For the upsloping bed the grounding line will advance more compared to the flat and downsloping bed and retreat the least. The downsloping bed will retreat by the largest amount but advance by the smallest amount compared to the flat and upsloping bed.

There doesn't appear to be any change in tendency of grid point evolution with the varying beds and the difference in grounding line position for different basal slopes is smaller than the initial grid size and so within the accuracy of the model, indicating that the model is independent of basal topography. This agrees with the results found in the Vieli and Payne survey paper [11] and the results of Hindmarsh [3].

Looking more closely at the upsloping bed we find that in contrast to the ice sheet instability hypothesis the ice thickness at the grounding line does not increase as the grounding line recedes but decreases. The moving mesh models in the Vieli and Payne paper also exhibit this behaviour.

The tendency for the ice thickness to decrease as the grounding line recedes is worrying as it is counter intuitive. As sea level remains constant in this model, when the grounding line recedes along an upsloping bed then the water depth would increase. If the ice height at the grounding line decreases then it would imply that the flotation criterion is no longer met. This could either indicate that there is a problem with the method or perhaps a problem with the modelling of the grounding line migration rate.

As mentioned before, the accumulation term in this dissertation includes the combination of the accumulation and ablation. In the methods discussed in the Vieli and Payne survey paper [11], even for a positive accumulation the grounding line can recede and the total mass can decrease. This would indicate that the mass is lost in another part of the method. If we make the assumption that the m in the grounding line migration equation is strictly the amount of accumulation with no contribution of ablation and allow $m(a(t))$ at the grounding line to be $0.1ma^{-1}$ as in the Vieli and Payne survey paper we still find that the ice height at the grounding line decreases as the grounding line recedes.

Further investigation into the grounding line migration rate exposes a key differ-

ence between the migration rate specified in the Vieli and Payne paper [11] and the Hindmarsh paper [3] that the migration rate was originally taken from. We have so far taken $f = l - h$ as in the Vieli and Payne paper, however in the Hindmarsh 1996 paper $f = l - b$. Differentiating the flotation criterion

$$\rho_i h = \rho_w (l - b)$$

gives

$$\begin{aligned} \frac{d}{dt}[\rho_i h] &= \frac{d}{dt}[\rho_w (l - b)] \\ \frac{\partial \rho_i h}{\partial t} + \frac{\partial x}{\partial t} \frac{\partial \rho_i h}{\partial x} &= \frac{\partial \rho_w (l - b)}{\partial t} + \frac{\partial x}{\partial t} \frac{\partial \rho_w (l - b)}{\partial x} \end{aligned} \quad (58)$$

Letting $f = l - b$, $v = \frac{\partial x}{\partial t}$ and dividing both sides by ρ_i we have

$$\begin{aligned} \frac{\partial h}{\partial t} + v \frac{\partial h}{\partial x} &= \frac{\rho_w}{\rho_i} \frac{\partial f}{\partial t} + v \frac{\rho_w}{\rho_i} \frac{\partial f}{\partial x} \\ v \left[\frac{\partial h}{\partial x} - \frac{\rho_w}{\rho_i} \frac{\partial f}{\partial x} \right] &= \frac{\rho_w}{\rho_i} \frac{\partial f}{\partial t} - \frac{\partial h}{\partial t} \\ v &= \frac{\frac{\rho_w}{\rho_i} \frac{\partial f}{\partial t} - \frac{\partial h}{\partial t}}{\frac{\partial h}{\partial x} - \frac{\rho_w}{\rho_i} \frac{\partial f}{\partial x}} \end{aligned} \quad (59)$$

Implementing this change exhibits some differences in the results. Firstly for an upsloping bed we find that as the grounding line recedes the ice at the grounding line thickens, confirming the results of Weertman [12] and Thomas and Bentley [8]. The flux for a final time of 15000 years, 21 grid points and $dt = 0.0025$, for all three basal slopes has been plotted in figure 7. We see a large variation in the flux in the first few time steps. This is due to the absence of initial conditions for the flux and so it takes a small amount of time for the flux values to settle down to their 'true' value. We allowed the model to run until the flux variations settled before we started plotting the flux.

The flux for the upsloping bed is much larger than for the downward sloping and flat beds. Even though the flux is much larger for an upsloping bed the grounding line migration remains stable. This can be seen in figure 9(b) where we can see that the grounding line recedes stably as the change in grounding line position decreases over time, with the change in grounding line position becoming less than $0.1ma^{-1}$ after 7500 years. This is because the flux does not increase with time but decreases. This would indicate that the flux is dominated by the velocity at the grounding line. The flux for a glacier in advance has been plotted for all three basal slopes in

figure 8. When the grounding line advances the ice thickness decreases, however for an upsloping bed we still see that the flux has the largest magnitude. Again, this indicates that the flux is dominated by the large velocity at the grounding line.

The reason for the larger fluxes for the upsloping bed is due to the large grounding line velocities. The f_x term now incorporates b_x in the new formula (59) for grounding line migration (59). For an upsloping bed this has the opposite sign to the downward sloping bed, the result of which is that the denominator of the grounding line migration equation is now much smaller and hence the grounding line migration is much larger.

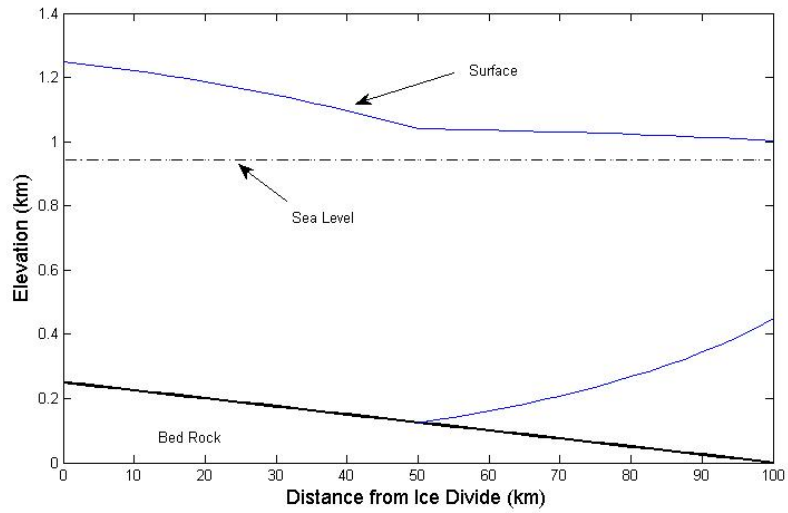
The grounding line position has been plotted in figure 9 for all three basal slopes using the new grounding line migration rate. The final time is 15000 years, there are 21 grid points, and $\Delta t = 0.0025$. Figure 9(a) has the accumulation set to $\int_0^{b(t)} m dx = 0.5ma^{-1}$. and figure 9(b) has the accumulation set to $\int_0^{b(t)} m dx = -0.5ma^{-1}$.

These figures show us that the change in grounding line position for different basal slopes is now much larger for the the new grounding line migration equation. This is in contrast to the Vieli and Payne paper where the grounding line migration should be independent of basal slope [11]. In addition the migration of the grounding line is now largest for an upsloping bed for both a receding and advancing glacier and smallest for a downsloping bed for both a receding and advancing glacier.

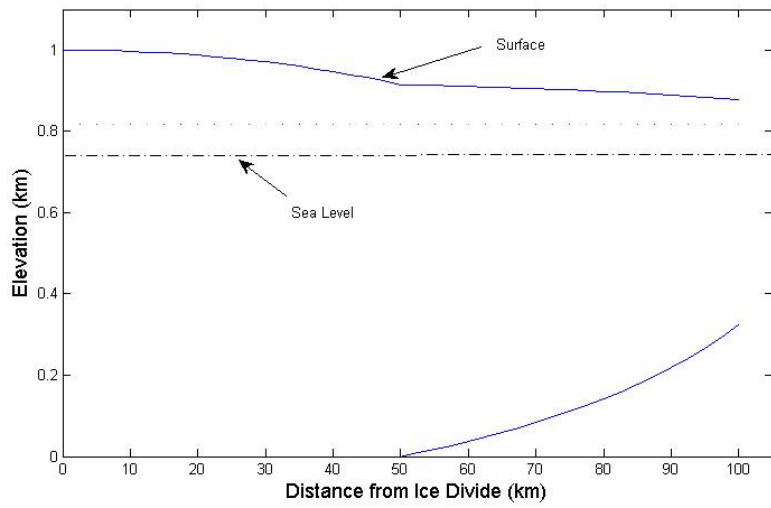
Another key feature of the new grounding line migration equation (59) is that for the downward sloping bed the grid points advance or recede by a smaller amount, while for an upsloping bed the grid points advance or recede by a much larger amount and for a flat bed the grid points also advance or recede by a larger amount. The grounding line migration has been plotted to illustrate this in figure 10. Also notice that for the old grounding line migration rate there was a tendency for the grounding line to initially recede for all basal slopes. This is further evidence that the old equation for the grounding line migration rate is not a good representation of the grounding line migration.

We tested the convergence of the model with the new equation for grounding line migration in the same way as in section 6.3 and found that the method was of approximately order 2.

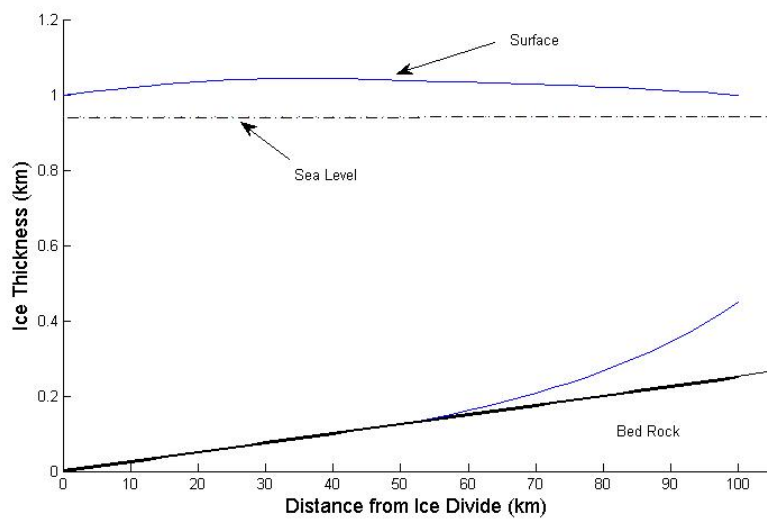
To conclude this discussion, the moving mesh method is stable for a glacier on all basal slopes, which agrees with the results found in the Vieli and Payne 2005 survey paper, and contradicts the theoretical arguments of Weertman (1974) and Thomas and Bentley (1978). However we find that grounding line migration does depend on the basal topography, which is in contrast to the results of Vieli and Payne [11].



(a) Downward Slope



(b) Flat Bed



(c) Upward Slope

Figure 6: Different Ice Bed Profiles

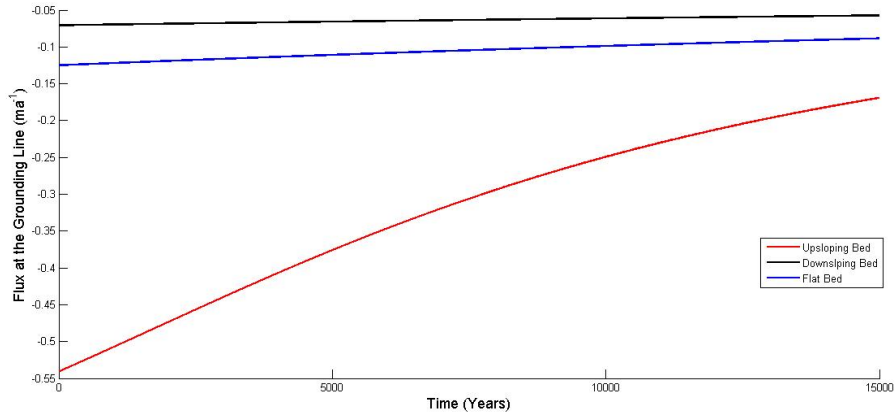


Figure 7: Flux at the Grounding Line for each basal slope with $\int_0^{b(t)} m dx = -0.5ma^{-1}$

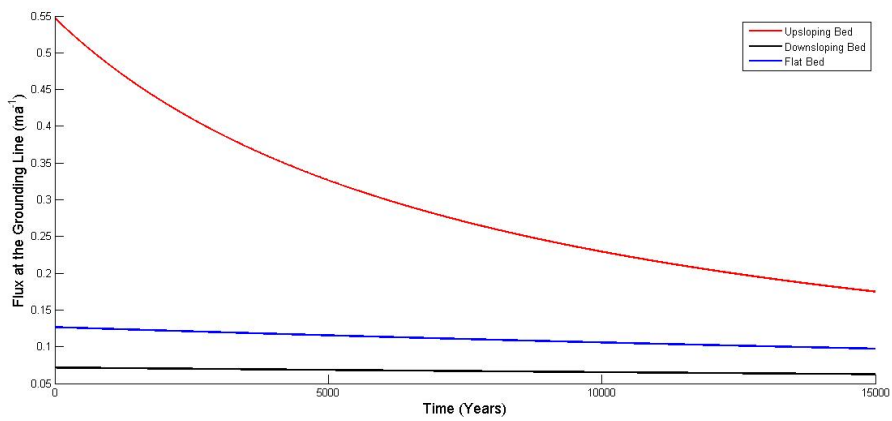
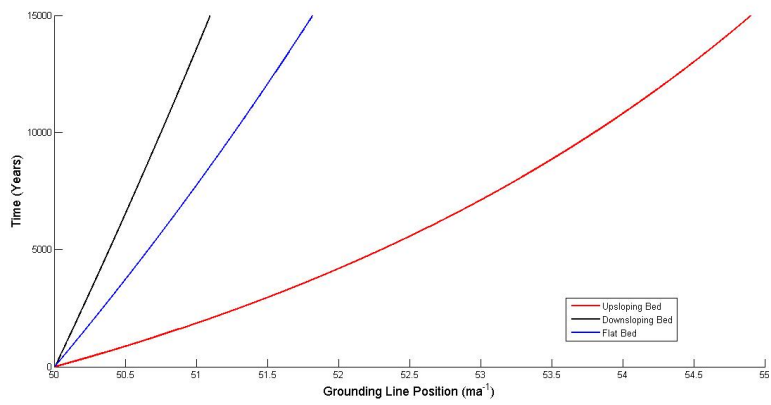
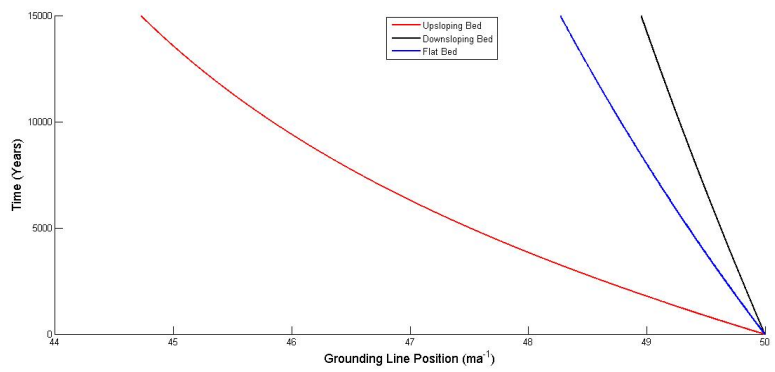


Figure 8: Flux at the Grounding Line for each basal slope with $\int_0^{b(t)} m dx = 0.5ma^{-1}$

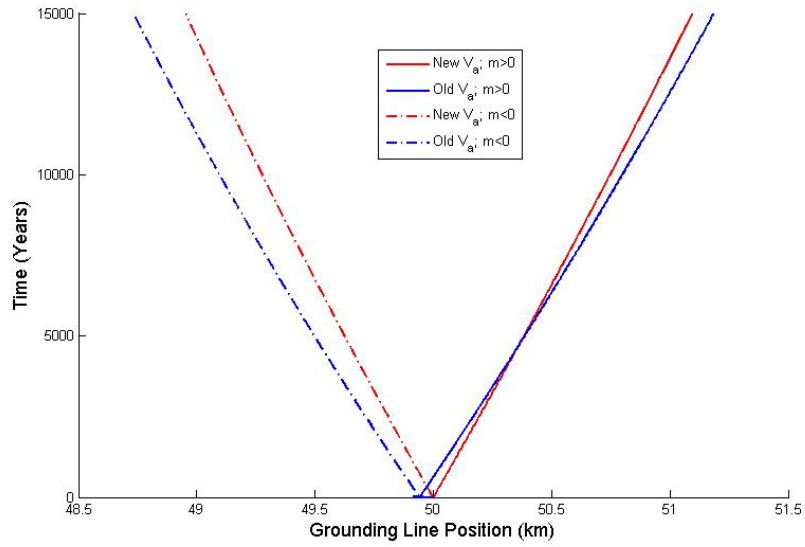


(a) Advancing Glacier

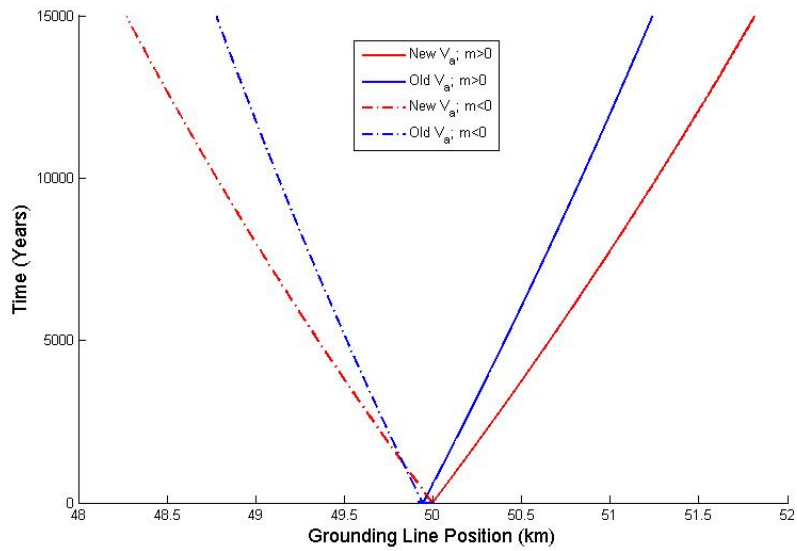


(b) Receding Glacier

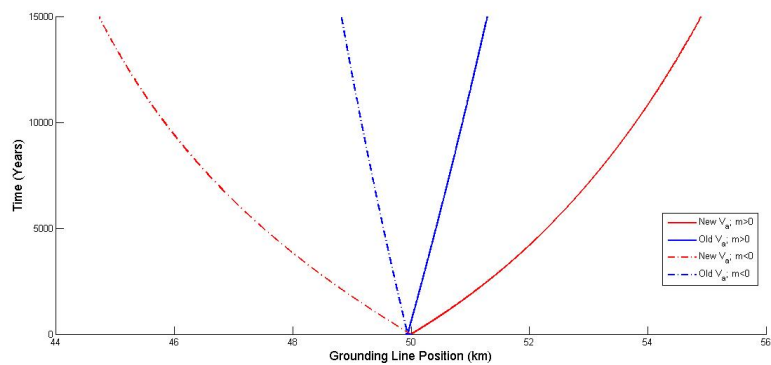
Figure 9: The grounding line position over 15000 years for different basal slopes



(a) Downward Slope



(b) Flat Bed



(c) Upward Slope

Figure 10: Comparison of the change in grounding line position between the new and old equation for grounding line migration for different basal slopes.

9 Changes to Sea Level

We allow the sea level to change by 5% over 1000 years, which amounts to a change of approximately $60m$. For this experiment there are 21 grid nodes and Δt is set to 0.000625, the net accumulation is set to $\int_0^{b(t)} m(x)dx = 0.3ma^{-1}$, which allows the initial profile to remain in approximate steady state. For a sea level rise of 5% the grounding line recedes by approximately $8.5km$. For a 5% decrease in sea level the grounding line advances by approximately $7.5km$. This is a much larger change than that described by the moving mesh models in the Vieli and Payne survey paper, where the grounding line position recedes by approximately $2km$ for a of sea level rise of $125m$ and advances by $1.5km$ for a decrease of sea level of $125m$. The grounding line migration of this method is also larger than the migration of the fixed grid methods of the Vieli and Payne paper. These differences could be attributed to the difference in the initial profile. For this dissertation we chose the sea level such that the flotation criterion was met at the mid point of the glacier. This is counter-intuitive as sea level determines the position of the grouning line and not vice versa. We chose this way as we wanted to replicate the conditions in the EISMINT experiments. Instead, if we allow the sea level to be $500m$ and obtain the expected position of the grounding line using the flotation criterion, we find that the resulting values for the migration of the grounding line are very different. Allowing the same changes to sea level as before gives an advance of less than $1km$ and a retreat of approximately $3.5km$.

Allowing the sea level to return to the original position over 1000 years exhibits a return to the original grounding line position indicating that changes to sea level are reversible.

10 Changes to Rate Factor

The rate factor A is strongly dependent on the temperature of the ice. The fixed grid models of the Vieli and Payne paper were strongly dependent on the rate factor and thus the modelled temperature of the ice. For the previous experiments of this dissertation the rate factor has been taken to be $A = 10^{-18}$, which corresponds to an ice temperature of $-34^{\circ}c$. This is rather too low to be realistic [11]. Increasing the rate factor corresponds to a decrease in the modelled ice temperature. It was found that an increase in ice temperature caused the fixed grid models to have a higher tendency to recede. For the moving mesh models in [11] the change in rate

factor had very little effect on the grounding line dynamics although the absolute values in grounding line change were larger [11]. For the moving mesh method of this dissertation a higher rate factor makes very little change to the grounding line. In an advancing glacier the difference in grounding line position is marginally larger for a higher rate factor. For a receding glacier the change in grounding line position is marginally smaller for the higher rate factor.

This indicates that this model is not very sensitive to the ice rheology; similar to the Vieli and Payne paper. This indicates that errors in the modelled ice temperature will not strongly affect the results.

11 Conclusion and Discussion

Accurate and efficient modelling of the grounding line in glaciology is crucial in order to make reliable forecasts of the fate of the Cryosphere. Changes to grounded ice in the Cryosphere will greatly impact upon the Earth's climate system. Recent rates of receding ice sheets has prompted an increase in the desire to properly understand the dynamics of these glaciers. The modelling of glacier dynamics has experienced considerable development in recent years. However the results thus far have been inconsistent.

One common feature in many recent studies, such as the MISMIP [5] and Vieli and Payne [11] survey papers is that moving mesh models are often more reliable and robust as they avoid interpolation at the grounding line and are therefore less dependent on the grid resolution.

This project has been concerned with assessing the practicality of the Conserved Mass Fractions (CMF) moving mesh method of Baines, Hubbard and Jimack [1]. This method forces local mass fractions to be preserved when moving the mesh. A benefit of this model is that local mass balance is respected, which is a key physical feature of glaciers.

In the introduction we set out to introduce the basic theory of glaciology and the motivation in modelling the migration of the grounding line. Throughout this dissertation we have covered several topics. These have been summarised here.

- In section 2 we defined the diffusive velocities for the sheet and shelf separately without coupling and without the accumulation term.
- In section 2.3 we discussed the numerical techniques used to approximate the diffusive velocities and how to advance the mesh using these velocities.
- Section 3 introduced the method of conservation of mass fractions in order to allow for variable mass in the sheet and shelf and in order to later incorporate the coupling between sheet and shelf.
- We defined the deformation velocity in section 3.2 and showed how these velocities are affected by the diffusive velocity and the velocity induced by the conserved mass fractions.
- In section 3.3 we discussed the modification to the numerical method for incorporating the mass fractions, and also the time stepping method we used to move the mesh with the approximated deformation velocity.

- Section 3.3.3 outlined an algorithm for the method so far.
- We then went on to discuss how we recover the new ice heights using mid-point approximations, made possible by the conserved mass fractions method.
- We reintroduced the accumulation term in section 4 and discussed how this affected the algorithm in section 3.3.3.
- In section 5 we discussed the necessity of non-dimensionalisation for application to real data and how we facilitated this necessity in the method.
- Section 6.1 investigated the steady state solution and found that our model achieves a near steady state, where h_t is sufficiently small, when the accumulation term is sufficiently small.
- Section 6.2 investigated how the viscosity ν affected the model and found that the difference between varying and constant viscosity is relatively small, however it does alter the tendency of the shelf front to advance or recede. Despite the very small difference in varying viscosity and constant viscosity, incorporating the varying viscosity is relatively easy and so it is preferable to include it, as constant viscosity is too crude an assumption to make.
- We tested for convergence in section 6.3 and showed that our method is convergent and approximately second order.
- We examined the dependency of the model on the number of nodes in section 6.5. We found that the method is reliable with a coarse resolution, as the method is not strongly reliant on the number of nodes. This demonstrated a robustness typical of moving mesh models.
- Section 7 investigated how changes to the accumulation affected the evolution of the glacier. We found that changes to the accumulation rate caused the glacier to evolve in a way that we would expect. For example, a positive accumulation caused the grounding line to advance and a negative accumulation caused the grounding line to recede. For a net accumulation of zero the grounding line position hardly changed. We also found that changes to the glacier incurred by changes in the accumulation were reversible. We found that the model is strongly dependent on the chosen accumulation rate, which is problematic as modelling the accumulation and ablation measurements can be inaccurate and so the inaccuracies in these measurements will present inaccuracies in the model.
- In section 8 we introduced an elevation to the ice bed. We discussed how this affected the design of the model, the effect the basal slope has on the glacier dynamics, and the stability of the model on different basal slopes. We found

that the CMF moving mesh method is stable for all basal slopes. However the the grounding line migration is dependent on basal topography.

- Section 9 investigated how the model reacts to changes to in sea level and found that changes in sea level affected the grounding line position in a way we would expect. For example a rise in sea level caused the grounding line to recede and a decrease in sea level caused the grounding line to advance. We also found that changes to the grounding line position incurred by changes in sea level were reversable.
- Finally, section 10 investigated how changes to Rate Factor A affected the model and the sensitivity of the model to ice temperature. We found that the model was not highly dependent on the rate factor and therefore insensitive to the modelled ice temperature.

The main aims of this dissertation have been to investigate the efficiency of the CMF moving mesh approach at modelling the migration of the grounding line and investigate how the behaviour of this model correlates with other schemes. We found that the model is convergent and we have been able to make favourable comparisons to the moving mesh models discussed in the Vieli and Payne survey paper [11], however our model does exhibit several distinct differences.

Firstly we see the grounding line recede for a small positive accumulation in the moving mesh methods described in the Vieli and Payne survey paper [11]. This is counter-intuitive as an increase in mass at the grounding line will give a larger mass to the ice and so would require more water to keep the ice bouyant. As sea level remains constant in these experiments we would expect more ice to become grounded. As this is not the case it demonstrates that the models in the Vieli and Payne paper do not fully respect true mass balance while the model used in this paper does. Mass conservation or mass balance is a key feature of glaciers.

Secondly we found that the model is stable for all basal slopes, which contradicts the results of Weertman [12] and Thomas and Bentley [8], as although the ice thickens as the grounding line recedes on an upsloping bed, the flux appears to be dominated by the grounding line velocity. A stable model for all basal slopes confirms the results of Hindmarsh [3] and the Vieli and Payne [11] survey paper. Although the grounding line is more dependent on the topography of the ice bed than stated in the Vieli and Payne paper, [11].

A caveat to this is that the CMF moving mesh model used in this paper is only one-dimensional. We also disregard full mechanical coupling with the ice stream and instead use only semi-coupling between the sheet and the shelf. There are also a number of other assumptions we have made in this model that may have large effects on the stability, such as assuming that there is no basal sliding. Extending the model

to include these factors may change the results.

To conclude, this dissertation is unique in the sense that we have used a moving mesh method based on conserved mass fractions with the addition of semi-coupling between the sheet and shelf. Dale Partridge [4] used the same moving mesh method for a grounded ice sheet without the addition of the semi-coupling between the sheet and the shelf. To have an increasing ice height for a receding glacier on an upward slope, an amendment to the flotation criterion described in the Vieli and Payne paper [11] needed to be made. This amendment allowed the ice height to increase as the glacier receded along an upward slope. This is required so that the flotation criterion is continued to be met, however the experiments in the Vieli and Payne paper did not exhibit this behaviour. Despite this change in the behaviour of the ice height we still found that the retreat of the grounding line was stable for an upsloping bed, contradicting the results of Hindmarsh [3] and [7]. However the grounding line dynamics are more dependent on the basal topography than suggested in the Vieli and Payne paper [11].

In addition we have found that the tendency of the grounding line to advance or recede is dictated by the sign of the net accumulation. This is in contrast to the Vieli and Payne paper [11] where a small positive accumulation led to a receding grounding line. This is potentially caused by the moving mesh models in the Vieli and Payne paper not being locally mass conserving.

11.1 Further Work

11.1.1 Full Stokes Equations

Many numerical models make use of the shallow ice approximations. These approximations use vertical averaging to simplify the full Stokes' equations. There have been relatively few attempts to model the ice dynamics with the full Stokes' equations, but one example of a model using the full Stokes' equations occurs in the MISMIP paper. It was found there that the results of the full Stokes' equations yielded much larger changes to the grounding line position. This model is however computationally costly and modelling the grounding line with the use of full Stokes' equations includes the question of available computer resources.

11.1.2 Higher-Dimensions

Extending the model to a 2D model generalises the shallow ice mass balance equation (1) to

$$h_t + \nabla \cdot (hu) = m$$

For the 1D model we have used a finite difference scheme described in sections 2.3 and 3.3. This has been feasible for the 1D model, but it would not be appropriate to extend this to a 2D model as finite difference methods are inflexible. In order to adapt the model to 2D model we could employ a finite element scheme as in [1].

An example of the CMF moving mesh scheme being used in a 2D case with a finite element approximation can be found in [4]. The method was used to investigate the behaviour of the ice sheet only, with no coupling to the attached shelf. It was found that the glacier was able to advance and retreat successfully with no node tangling and that the results with this scheme had an increased accuracy compared to the moving mesh models used in the EISMINT scenario. However, the computational cost of running the model was greatly increased.

Incorporating finite elements has the added benefit that we can incorporate an unstructured triangular mesh. This would allow us to fit the numerical grid to a non-uniform domain. As glaciers aren't so considerate that they fit themselves neatly into square grids; a finite element method will allow us to model the glacier with more accuracy, as we can adjust the mesh to fit the domain.

Further work could be to investigate how the semi-coupled model behaves when incorporating the finite element method in 2D.

11.1.3 Ice Calving at the Shelf Front

Glaciers experience a sudden amount of mass loss at the shelf front due to ice calving. This is where large chunks of ice break from the shelf at the shelf front and float unattached to the glacier. This is a very efficient ablation mechanism. It has been found that the amount of melting at the grounding line is small compared to the mass loss by calving [10]. This clearly makes it a very important process, but it is still poorly understood.

Incorporating ice calving into the model could be problematic as it requires knowing at which point the ice will break off and when. It has also been suggested that finding a rate for calving for a floating ice shelf "may be illusory" [9]. As ice calving has such a large effect on the ice shelf and in turn the ice shelf can affect the grounding line, a better understanding of ice calving on floating ice shelves will lead to a better understanding of the migration of the grounding line.

Other extensions include incorporating basal sliding, investigating a time dependent accumulation rate and also to investigate full mechanical coupling between the ice sheet and ice shelf via the inclusion of an ice stream.

References

- [1] Baines, M. J. , Hubbard, M. E. and Jimack, P. K., Velocity-based moving mesh methods for nonlinear partial differential equations. *Communications in Computational Physics*, 10(3):509576 (2011)
- [2] Goldberg, D., Holland, D. M. and Shoof, C., Grounding Line Movement and Ice Shelf Buttressing in Marine Ice Sheets, *J Geophys. Res.*, Vol 114, doi:10.1029/2008JF001227 (2009)
- [3] Hindmarsh, R.C.A, Stability of Ice Rises and uncoupled marine ice sheets, *Ann. Glaciol.*, 23, 105-115 (1996)
- [4] Partridge, D., Numerical Modelling of Glaciers: Moving Meshes and Data Assimilation, PhD Thesis, University of Reading, UK (2013)
- [5] Pattyn, F., Schoof, C., Perichon, L., Hindmarsh, R. C. A., Bueler, E., de Fleurian, B., Durand, G., Gagliardini, O., Gladstone, R., Goldberg, D., Gudmundsson, G. H., Lee, V., Nick, F. M., Payne, A. J., Pollard, D., Rybak, O., Saito, F., and Vieli, A.: Results of the Marine Ice Sheet Model Intercomparison Project, MISMIP, *The Cryosphere Discussion*, Vol 6, 267-308, doi:10.5194/tcd-6-267-2012 (2012).
- [6] Shepherd, A. and Wingham, A., Recent Sea-Level Contributions of the Antarctic and Greenland Ice Sheets, *Science*, 315, 1529-1532 (2007).
- [7] Schoof, C., Marine ice-sheet dynamics. Part 1. The case of rapid sliding. *Journal of Fluid Mechanics*, 573:27 (2007)
- [8] Thomas, R. Bentley, C. Model for Holocene retreat of the West Antarctic Ice Sheet. *Quaternary Res*, 10(2), pages 150-170.(1978)
- [9] Van Der Veen, C.J., Tidewater Calving. *Journal of Glaciology* Vol. 42, No 141 (1996)
- [10] Vieli, A., Jania, J. and Kolondra, L., The retreat of a tidewater glacier: observations and model calculations on Hansbreen, Spitsbergen. *Journal of Glaciology* Vol. 48, No 163, (2002)
- [11] Vieli, A. and Payne, J., Assessing the ability of numerical ice sheet models to simulate grounding line migration. *Journal of Geophysical Research*, Vol. 110, (2005)

- [12] Weertman, J. Stability of the junction of an ice sheet and an ice shelf. *J. Glaciol. Journal of Glaciology* Vol. 13, 3-11, (1974)